Open Ceramics 9 (2022) 100234

Contents lists available at ScienceDirect

Open Ceramics

journal homepage: www.sciencedirect.com/journal/open-ceramics

Effect of incorporation of piezoelectric phases on antibacterial and cellular response of borate bioactive glass

Angaraj Singh, Priya Singh, Ashutosh Kumar Dubey *

Department of Ceramic Engineering, Indian Institute of Technology (BHU) Varanasi, 221005, India

ARTICLE INFO

Keywords:
Borate bioactive glass
$BaTiO_3$
$Na_{0.5}$ $K_{0.5}$ NbO_3
Polarization
Antibacterial response

ABSTRACT

The present study investigates the consequences of incorporation (30 vol %) of piezoelectric $Na_{0.5}K_{0.5}NbO_3$ (NKN) and $BaTiO_3$ (BT) phases and surface polarization (20 kV at 500 °C) on *in-vitro* antibacterial and cellular response of borate bioactive glass (1393B3, BBG). XPS analyses elucidated that the surface chemistry of optimally processed composites remains unaffected after surface polarization treatment. The piezoelectric BT and NKN enhance the antibacterial activity of BBG by ~ (53, 57%) and (51, 54%) for *E. coli* and *S. aureus* bacteria stains, respectively. The SEM images of bacteria, adhered on unpolarized and polarized surfaces demonstrate bacteria specific response. The combined action of piezoelectric phase and surface polarization increases the growth rate of osteoblast like MG-63 cells on negatively polarized BBG- BT (30 vol %) and BBG- NKN (30 vol%) composites by ~ 76 and 82% respectively. Overall, the piezoelectric secondary phase incorporated in BBG as well as surface polarization increases the cellular and antibacterial response significantly.

1. Introduction

In the last few decades, remarkable research efforts have been made towards the development of novel biomaterials to regenerate the functional tissues in the fields of prosthetic dental care and reconstructive plastic surgery [1]. Such studies attempted to develop a biocompatible implant which can influence gene expression, osteogenic differentiation, cellular proliferation etc. after dissolution in the extracellular matrix [2]. Bioactive glasses such as, 45S5, 1393 etc. are widely used in orthopedic applications due to their reasonable bioactivity and osteoconductivity [3–6]. Such glasses make strong bond with soft tissues and bone, *in vivo* [7]. The bioactive glasses, such as 1393 and 45S5 support osseointegration, angiogenesis and bone regeneration [8]. However, these bioactive glasses gradually and partially convert into bone-like apatite crystals during *in-vitro* bioactivity tests [9]. The development of borate bioactive 1393 B3 glass became an efficient alternative for silicate-based bioactive glasses in the field of biomaterials [10]. The boron content in such bioactive glass rapidly alters the reaction rate [11]. The borate bioactive glasses attracted significant attention due to their rapid formation/growth ability of bone-like apatite than silicate-based bioactive glasses [12]. Furthermore, it has been demonstrated that borate-based glasses promote healing, differentiation and cell proliferation [13]. However, the risk of infection is quite high in most of the bioactive glasses. The bacterial infection causes complications in ~2.5% of knee and hip replacement surgeries and ~10% of joint replacement surgeries [14]. To overcome such serious issue, modification on reactive properties of bioactive glasses has been made to prevent microbial colonization and subsequent implant failure [15]. The incorporation of metal ions such as zinc, copper and silver etc., in bioactive glass enhances the antibacterial properties [16]. The incorporation of Ag (3 wt %) in 76S bioactive glass increases the antibacterial response against *Escherichia coli (E. coli)* by releasing the Ag^+ ions, which interact with the outer lipopolysaccharides layer of bacterial cells and damage the outer membrane [17]. It has been observed that doping of Cu ions in mesoporous bioactive glass increases the antibacterial efficiency (~75%) against *E. coli* (gram-negative) bacteria, after 24 h of incubation [18]. However, excess amount of these antibacterial modifiers can change the reaction rate of bioactive glass [19]. It has been demonstrated that borate-based bioactive glass has inherent antibacterial property as compared to silicate-based bioactive glass [20]. The presence of borate (B_2O_3) in B3 bioactive glass is enough to reduce the bacterial infection [21]. However, the potentiality of borate bioactive glass as antibacterial material remains unclear due to lack of sufficient data [22]. In another study, it has been reported that incorporation of 15 wt % silicate based bioactive glass in resin-based dental composite reduces the bacterial penetration by ~28%. However, for borate

* Corresponding author.
E-mail address: akdubey.cer@iitbhu.ac.in (A.K. Dubey).

https://doi.org/10.1016/j.oceram.2022.100234
Received 24 December 2021; Received in revised form 10 February 2022; Accepted 11 February 2022
Available online 22 February 2022

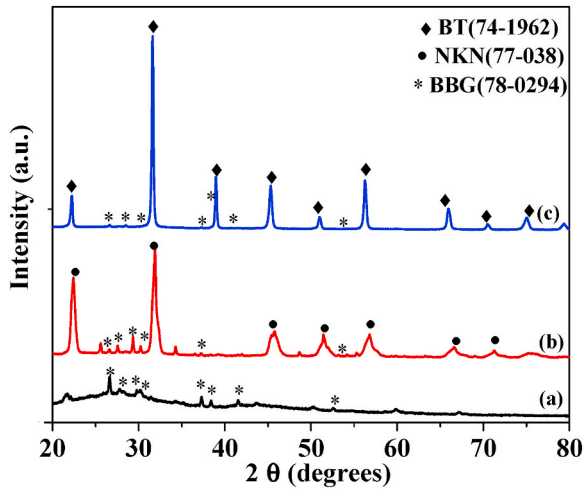

Fig. 1. The XRD patterns for sintered (a) BBG, (b) BBG-30 vol % NKN and (c) BBG-30 vol % BT composites.

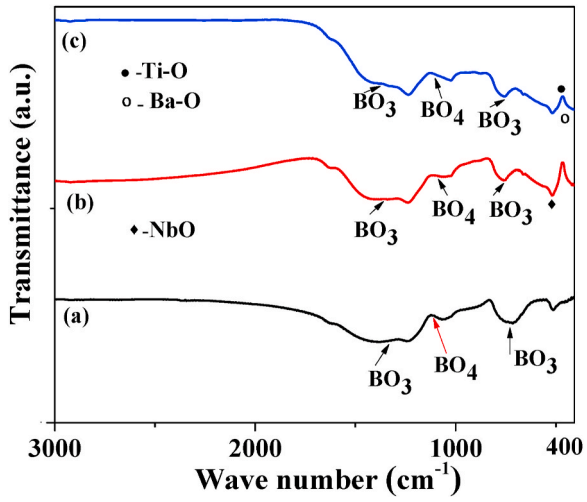

Fig. 2. FTIR spectra of sintered (a) BBG, (b) BBG-30 vol % NKN and (c) BBG-30 vol % BT composites.

bioactive glass, it is reduced by ~43% [23]. To overcome such issue, various antibiotics have been used during/after surgery to stop the bacterial colonization [24]. In orthopedic surgery, PMMA (poly methyl methacrylate) cement generally complied as antibiotic carrier to prevent bacterial infection. However, non-biodegradable PMMA deliver a surface for secondary bacterial infection [25].

Recently, piezoelectric sodium potassium niobite ($Na_{0.5}K_{0.5}NbO_3$) and barium titanate ($BaTiO_3$) has been incorporated in hydroxyapatite (HA) to improve the antibacterial as well as cellular properties [26–29]. It has been reported that the incorporation of piezoelectric phase enhances the proliferation of osteoblast-like cells on polarized 1393 bioactive glasses by ~78%, after incubation of 7 days [30]. In this perspective, the present study demonstrates the influence of addition of NKN and BT (30 vol %) as secondary phase in borate bioactive glass (1393B3, BBG) on *in-vitro* cellular and antibacterial response. In addition, the effect of polarization on surface chemistry of processed composite system was examined using XPS. The polarization induced cellular as well as antibacterial response was also examined. Towards the end, the mechanisms, responsible for cellular as well as antibacterial response, have been discussed.

2. Materials and methods

2.1. Materials synthesis

2.1.1. Synthesis of borate bioactive glass (1393 B3)

Borate bioactive glass, 1393B3 (BBG) with composition of 56% B_2O_3, 5.5% Na_2O, 18.5% CaO, 11.1% K_2O, 3.7% P_2O_5, 4.6% MgO was prepared using melt quench method. For this synthesis, MgO (99% assay, Loba Chemie, $CaCO_3$ (99% assay, Loba Chemie), Na_2CO_3 (99% assay, Sigma Aldrich), K_2CO_3 (99% assay, Sigma Aldrich), (NH_4) H_2PO_4 (99% assay, Loba Chemie) and boric acid (99.5% assay, Loba Chemie) were used as raw materials. Initially, stoichiometric amounts of each reagent were mixed in mortar pestle. Following this, the mixed powder was melted at 1300 °C/2 h. The melted slurry was then quenched in deionized water at room temperature. The obtained glassy samples were dried at 100 °C/12 h and then ball milled for 16 h in ethanol with zirconia balls to get the bioactive glass powder.

2.1.2. Synthesis of BBG -BT and BBG -NKN composites

The composites of BBG-x BT and BBG-x NKN (x = 30 vol %) were developed using solid state mixing route. BBG powder was mixed with NKN and BT powders separately and roll milled (using ethanol as milling medium) for 12 h at 600 rpm. Following this, the mixture was dried at 100 °C. The dried cake was then crushed in mortar pestle to obtain the powder. The pellets of 12 mm diameter were prepared using uniaxial hydraulic pressing machine and the green samples were sintered at 650 °C/10 min. The sintered pellets were polished for various characterizations.

2.2. Phase identification and microstructural analyses

The phase verification of the sintered compacts was done using X-ray diffraction (Rigaku Miniflex II Diffractometer, Cu-kα, XRD) method between the range of 20–80°. In addition, the Fourier transform infrared (FTIR) spectra (Bruker, Model Tensor 27, Germany, Spectrometer) was recorded between the range of 3000–400 cm^{-1}. The scanning electron microscope (SEM, Zeiss, EVO 18 Research) was used forexamining the surface morphology of BBG, BBG-NKN/BT (30 vol %) composite samples.

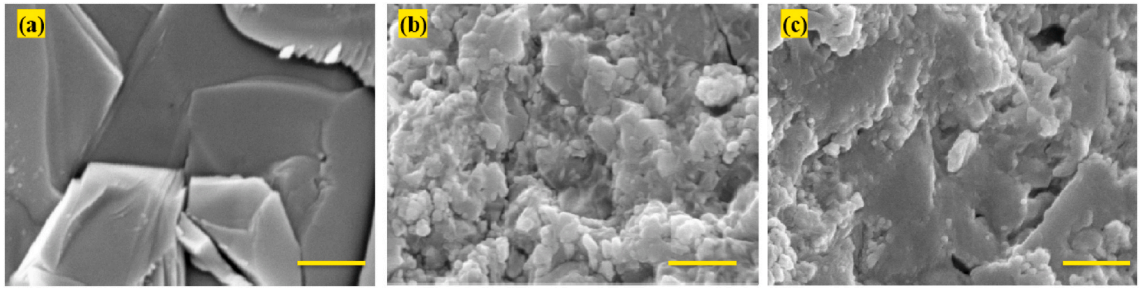

Fig. 3. SEM images of fractured (a) BBG, (b) BBG-30 vol % NKN and (c) BBG-30 vol % BT composites. Scale bar corresponds to 2 μm.

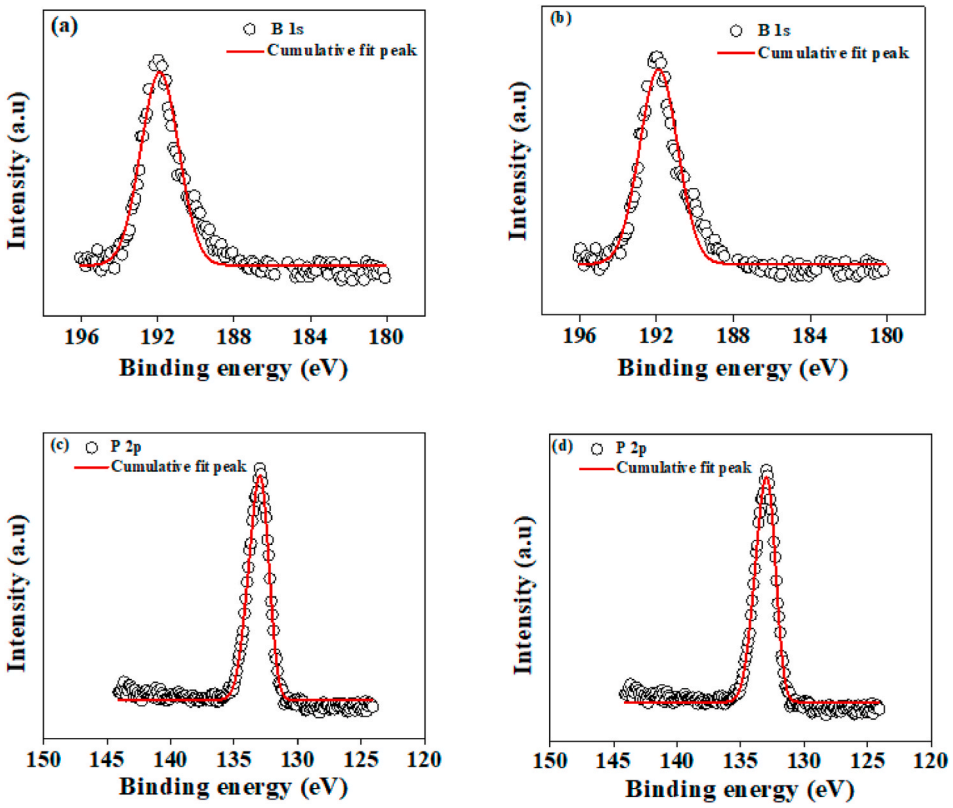

Fig. 4. The obtained and Gaussian fitted XPS spectra for unpolarized and polarized BBG (a, b) B 1s spectra, (c, d) P 2p spectra, (e, f), K 2p, (g, h) Ca 2p, (i, j) C, (k, l) O 1s, (m, n) Mg 1s, (o, p) Na 1s spectra, respectively and q represents the obtained XPS spectra for unpolarized and polarized BBG.

2.3. Electrical polarization

The sintered and polished pellets of BBG and BBG- NKN/BT (30 vol %) composites were poled using high temperature corona poling setup. The polarizing temperature and voltage were set to be 500 °C and 20 kV, respectively. The samples were heated up to 500 °C and a polarizing voltage of 20 kV (for 30 min) was applied. Thereafter, the samples were left in the chamber with the exposure of similar electric field, till it reaches to room temperature.

2.4. X-ray photoelectron spectroscopy (XPS)

The XPS analyses was done to observe the effect of surface polarization on surface chemistry of prepared BBG/BBG-30 vol % NKN/BT composites. The XPS of unpolarized and polarized samples were performed using X-ray photoelectron spectrometer system.

2.5. In-vitro antibacterial response

The gram-negative [*Escherichia* (*E.*) *Coli*] and gram-positive [*Staphylococcus* (*S.*) *Aureus*] bacteria were obtained from Chandigarh (Microbial Type Culture Collection), India. The procured bacteria were revived in their respective growth media (nutrient broth) before seeding [26].

2.5.1. MTT assay

MTT [3-(4, 5-dimethylthiazol-2-yl)-2,5-diphenyl tetrazolium bromide] assay generally used to quantitatively assess the antibacterial response of developed samples. The unpolarized substrates were autoclaved at 121 °C of temperature and 20 psi of pressure for 30 min. The polarized samples were sterilized with ethanol (70%) and washed with 1x PBS (phosphate buffer saline), before seeding. The sterilized pellets were cultured in 24 well plates with 200 μL of bacterial culture. After this, 500 μl of culture media was added. The bacterial cultured pellets were incubated for 8 h at 37 °C. After incubation, the culture media was removed and pellets were washed twice with 1x PBS. The equal amounts (500 μl) of reconstitute MTT (1:10 in PBS) was added in each well and further incubated at 37 °C for 2 h. The MTT solution was replaced with solvent [(500 μl of dimethyl sulfoxide (DMSO)] from each well to dissolve purple color formazan crystals [31]. The absorbance of solution (DMSO) was measured using ELISA microplate reader (Bio-red) at 595 nm [26]. The statistical analyses were performed using SPSS 20 software at statistically significant value, $p \leq 0.05$.

2.5.2. Live/dead ratio

Live/dead ratio suggests the ratio of viability of live to dead cells using the absorbance, measured in MTT assay [32]. The percentage of viable cells were calculated as,

$$\textbf{Viability}\ (\%) = \frac{\textbf{mean absorbance of the samples}}{\textbf{mean absorbance of control}} \times 100 \quad (1)$$

The live/dead ratio for *E. Coli* and *S. Aureus* bacteria was calculated as [26],

$$\textbf{live} \Big/ \textbf{dead ratio} = \frac{\textbf{Live cells}\ (\textbf{viability}\ \%)}{1 - \textbf{live cells}\ (\ \textbf{viability}\ \%)} \quad (2)$$

2.5.3. Nitro blue tetrazolium (NBT) assay

The produced superoxide anions (reactive oxygen species) were quantified using NBT assay [33]. The unpolarized and polarized BBG-x NKN/BT (x = 30 vol %) composites were cultured with *E. coli* and *S. aureus* bacteria. Further, NBT was added and incubated again for 1 h. The obtained blue colored precipitate was dissolved in DMSO solution and the absorbance was recorded at 595 nm [34,35].

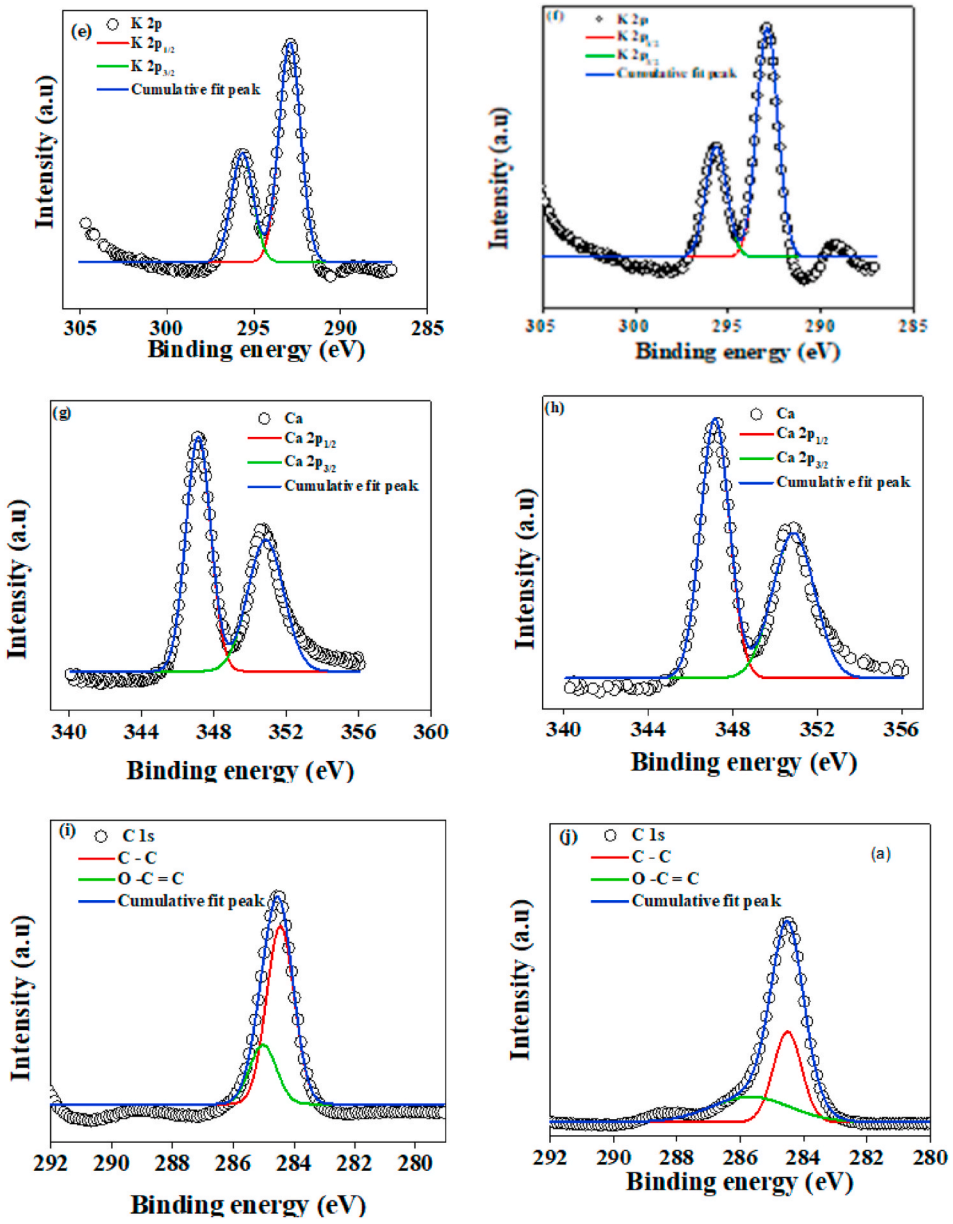

Fig. 4. (*continued*).

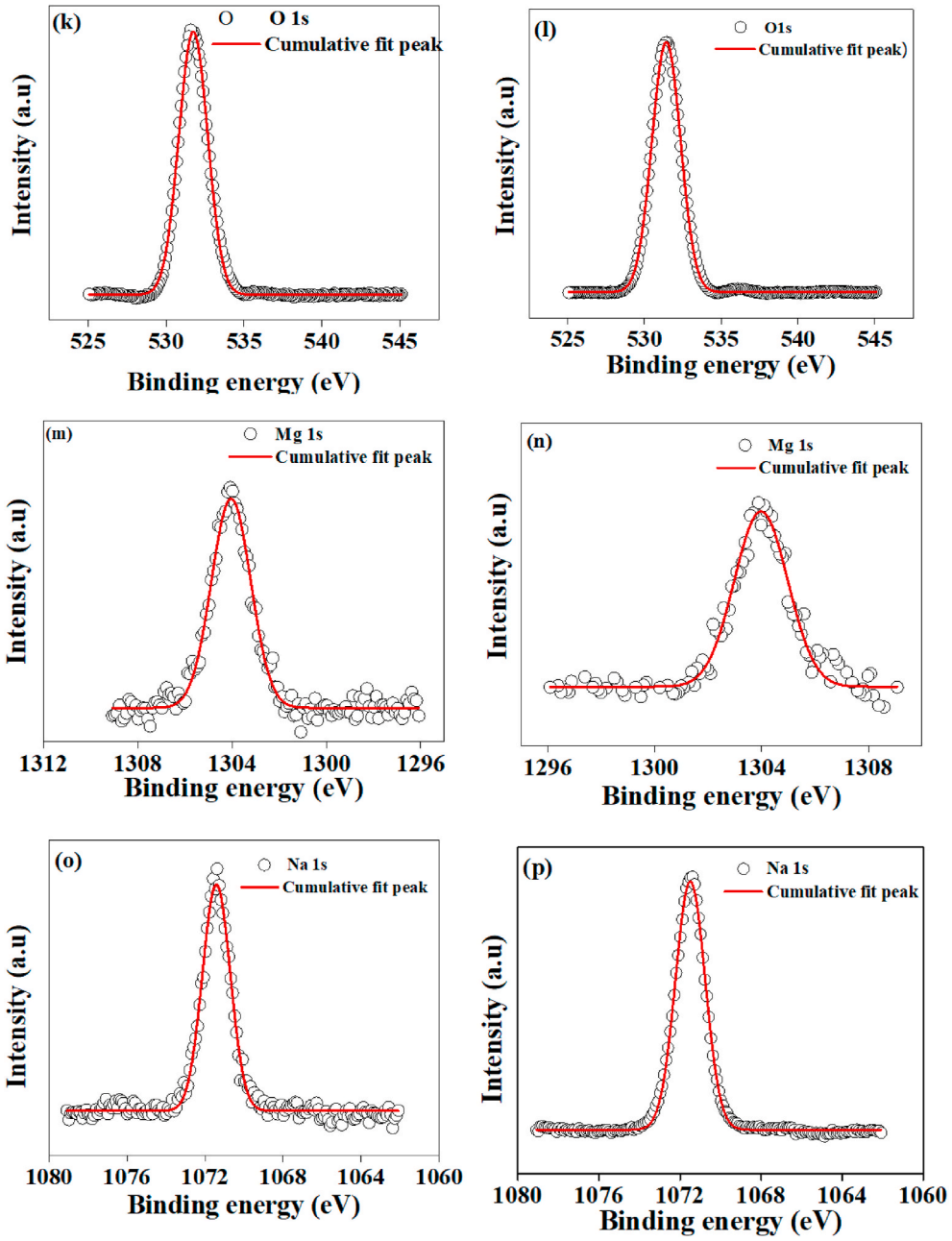

Fig. 4. (*continued*).

2.5.4. Bacterial adhesion test

The adhesion of *E. coli* and *S. aureus* bacteria, cultured on BBG-x BT/NKN (x = 30 vol %) composites was observed using SEM. Sterile samples of BBG-x NKN/BT composites were seeded with 200 μl diluted bacterial strain and incubated for 12 h. Thereafter, the samples were washed thrice with 1 x PBS. After this, 0.25% gluteraldehyde was added (for 30 min) to fix the cells on solid substrate. The samples were then washed thrice with 1 x PBS. After this, the bacterial cells, adhered on the samples were dehydrated using ethanol series of 30%, 50%, 70%, 90%, and 100%. The dried samples were coated with gold to examine under SEM.

2.6. In-vitro cellular response

For *in-vitro* cellular response, MG-63 cells were procured from NCCS (National Centre for Cell Science) Pune, India. The cells were cultured in DMEM (Dulbecco's modified Eagle's medium), 15% FBS (fetal bovine serum) and 1% antibiotics. The cultured cells were incubated in humidified CO_2 (5%) incubator (Thermo scientific Heracellvios 160i CO_2 incubator) at 37 °C. After incubation, trypsin was added to detach the adhered cells from the flask wall, which was counted using hemocytometer. The sterilized samples were seeded with 10^4 cells and left for

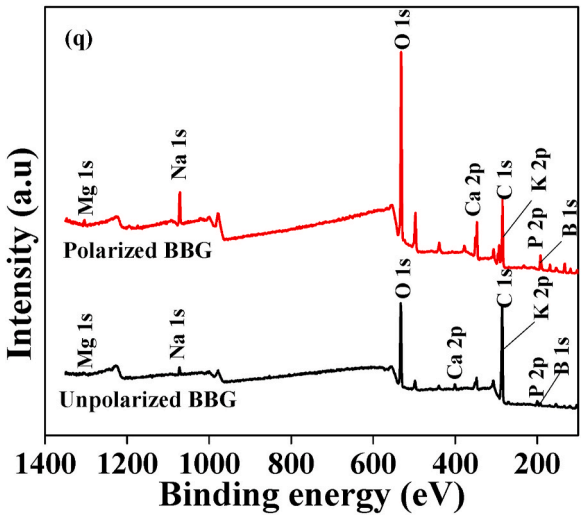

Fig. 4. (*continued*).

30 min in biosafety cabinet. Following this, 500 μL of respective growth media were added and incubated for 3, 5 and 7 days.

2.6.1. MTT assay

MTT assay measures the viability of MG-63 cells, according to ISO 10993-5 standard. The MG-63 cells (10^4 cells) were added with respective media in 24 well plate containing dried samples. The samples were incubated in CO_2 incubator for 3, 5 and 7 days, respectively. Following this, 1x PBS was added to wash the samples which was further incubated with reconstituted MTT. The formazan crystals were dissolved in dimethyl sulfoxide. The absorbance of obtained solution was measured at 595 nm using ELISA micro plate reader, which indicates the viability of live cells. The viability of MG-63 cells was calculated as [36],

$$\textbf{Cell viability} = \frac{\textbf{Mean absorbance of sample}}{\textbf{Mean absorbance of control}} \times 100 \quad (3)$$

2.6.2. Morphological analyses

Polarization induced morphological change of MG-63 cells was examined using fluorescent microscope (Nikon Eclipse LV 100 ND). The sterilized samples were seeded with 10^4 cells/well and incubated in CO_2 incubator for 3 days at 37 °C. After incubation, the cells were fixed with paraformaldehyde (30 min, 3.7%). The cells were permeabilized by Triton X-100 and blocked with BSA (bovine serum albumin). Alexa Fluora (488 Phalloidin) and DAPI fluorescent dyes were used for staining the cytoskeleton and nucleus of cells, respectively, as per the standard protocol.

3. Results and discussion

3.1. Phase identification and microstructural analyses

The XRD patterns of sintered BBG, BBG-30 vol % NKN and BBG-30 vol % BT composite samples are represented as Fig. 1. The XRD patterns were analyzed using X-pert high score software and indexed as per the standard JCPDS data. The XRD analyses revealed the formation of phase pure BBG (monoclinic), NKN (monoclinic) and BT (tetragonal) samples [27,29,37]. In case of composite samples, characteristic peaks of BBG, NKN and BT were observed without any reaction between the constituent phases.

Fig. 2 represents the FTIR spectra of sintered powder samples of BBG, BBG-30 vol % NKN/BT compositions. The broad resonances, known for borate bioactive glass network, are observed in the range of 1350–1450 cm^{-1}, 900–1100 and 690-720 cm^{-1} [Fig. 2(a)]. The bending and stretching (B–O) modes of vibration for BO_3 groups are appeared at 1350- 1450 cm^{-1} and 690-720 cm^{-1}, respectively. Whereas, the band appears at 900-1100 cm^{-1} attributes the stretching (B–O) of BO_4 groups. The broad resonance of NbO at ~524 cm^{-1} [Fig. 2 (b)] confirms the presence of NKN in BBG-30 vol % NKN composite. The presence of Ti–O and Ba–O bands in the FTIR spectra of BBG-30 vol % BT composite [Fig. 2 (c)] confirms the presence of BT in composite samples. The resonance appeared at 592 and 452 cm^{-1}, correspond to bending and stretching vibrations of Ti–O, respectively [26,38]. However, vibration of Ba–O bands is observed at ~430 cm^{-1} [39].

Fig. 3 represents the morphology of fractured BBG and BBG-30 vol % NKN/BT composite samples. Brittle mode of fracture has been observed for all the composites. Also, the densification of BBG composites is observed to increase with addition of secondary phases.

3.2. X-ray photoelectron spectroscopy (XPS) analyses

The XPS patterns of BBG samples are shown as Fig. 4 The binding energies of associated elements such as B, P, K, Ca, C, O, Mg and Na were analyzed before and after polarization. The binding energy of B was measured to be ~191 eV as B 1s spectrum for both, unpolarized and polarized BBG samples [Fig. 4 (a, b)] [40]. The peak, corresponds to P 2p spectrum, shows the binding energy of 135 eV for both, unpolarized and polarized BBG samples [Fig. 4 (c, d)] [41]. The K 2p spectrum shows two different binding energies (K $2p_{1/2}$–295.4 eV) and K 2p $_{3/2}$–292.6 eV) [Fig. 4 (e, f)] [42]. Similarly, Ca 2p spectrum was deconvoluted into two

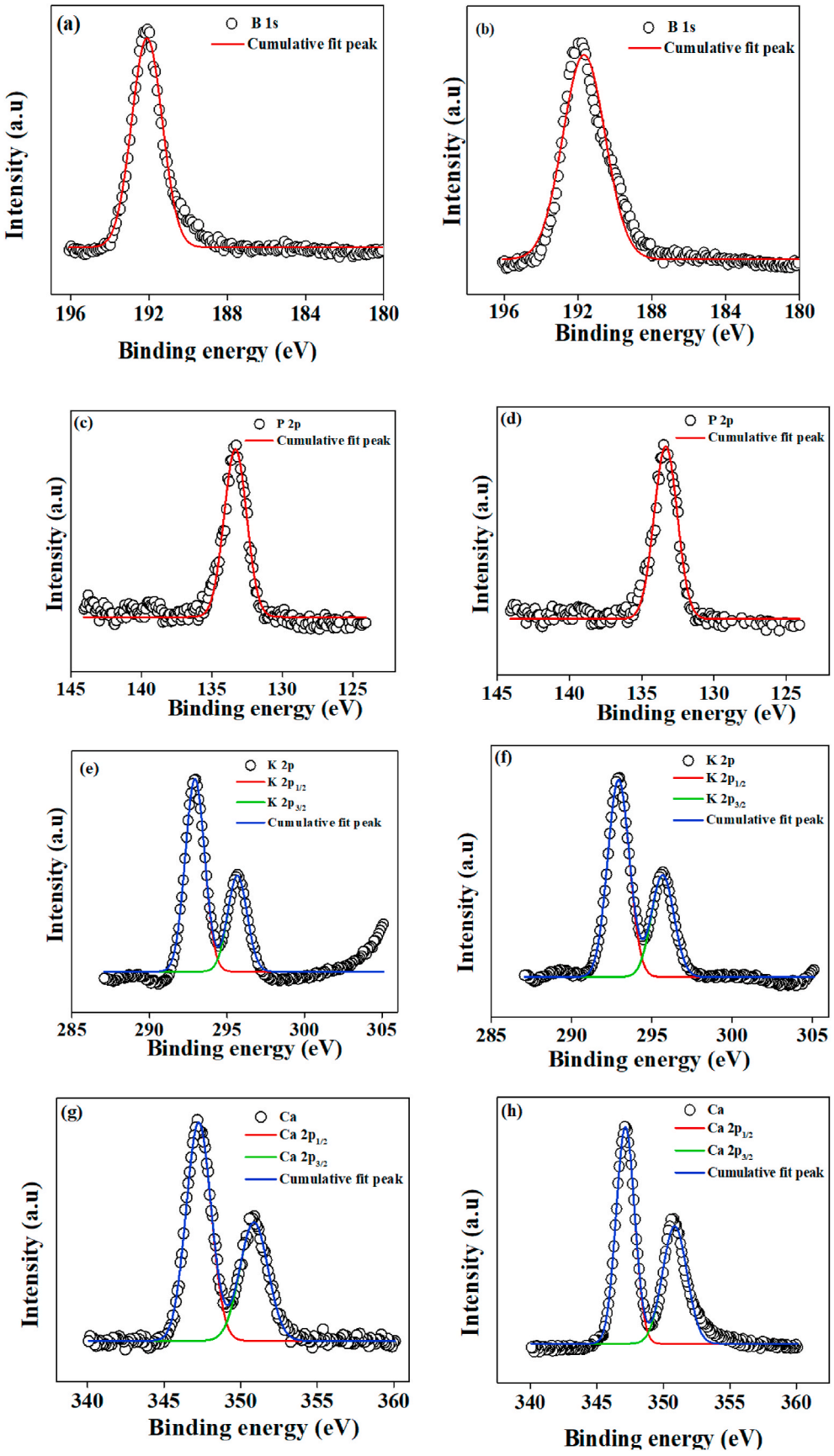

Fig. 5. The obtained and Gaussian fitted XPS spectra for unpolarized and polarized BBG- 30 vol% NKN composite (a, b) B 1s spectra, (c, d) P 2p spectra, (e, f), K 2p, (g, h) Ca 2p, (i, j) C, (k, l) O 1s, (m, n) Mg 1s, (o, p) Na 1s, (q, r) Nb 3d spectra and (s, t) represent the combination of all obtained XPS spectra for unpolarized and polarized BBG, respectively.

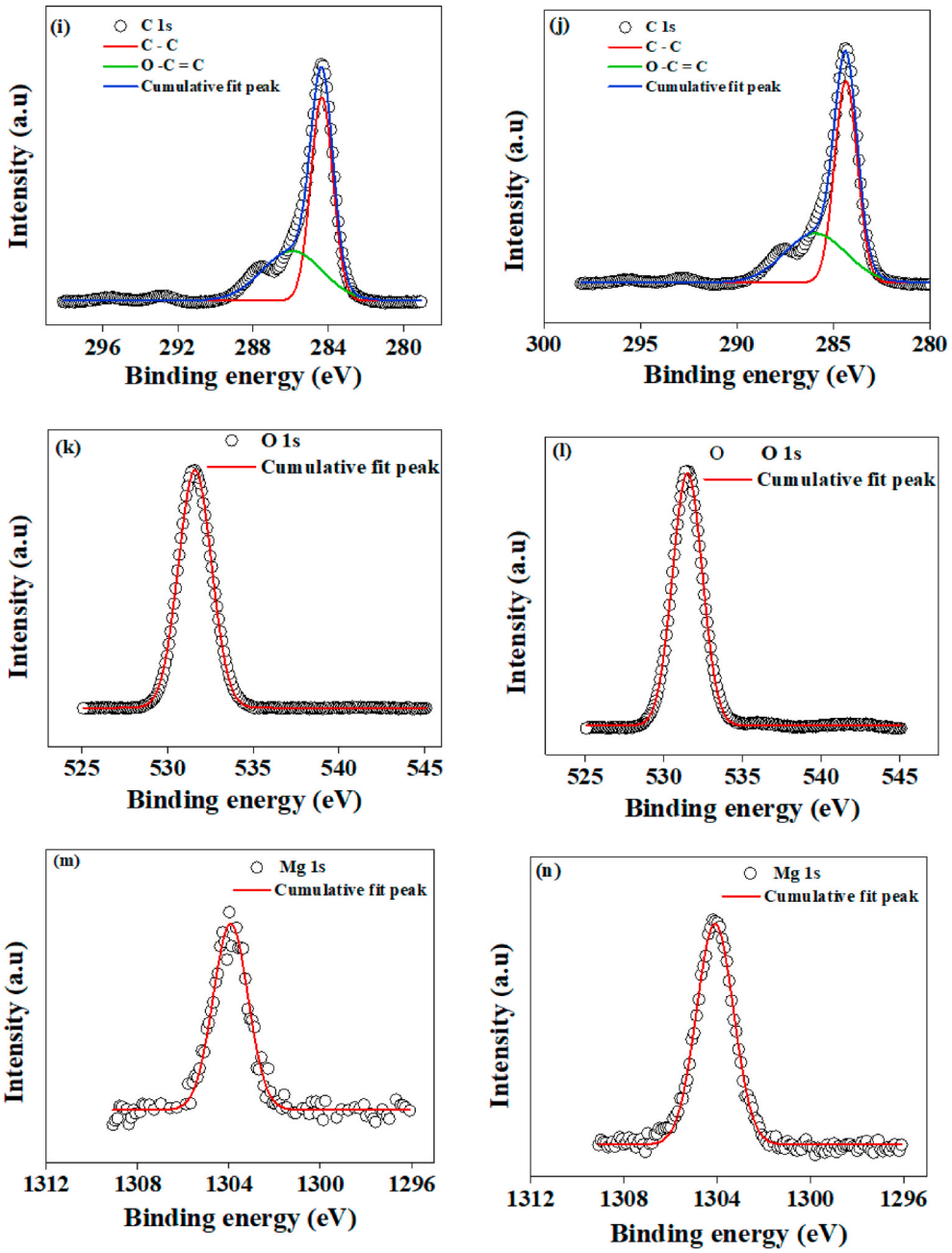

Fig. 5. (*continued*).

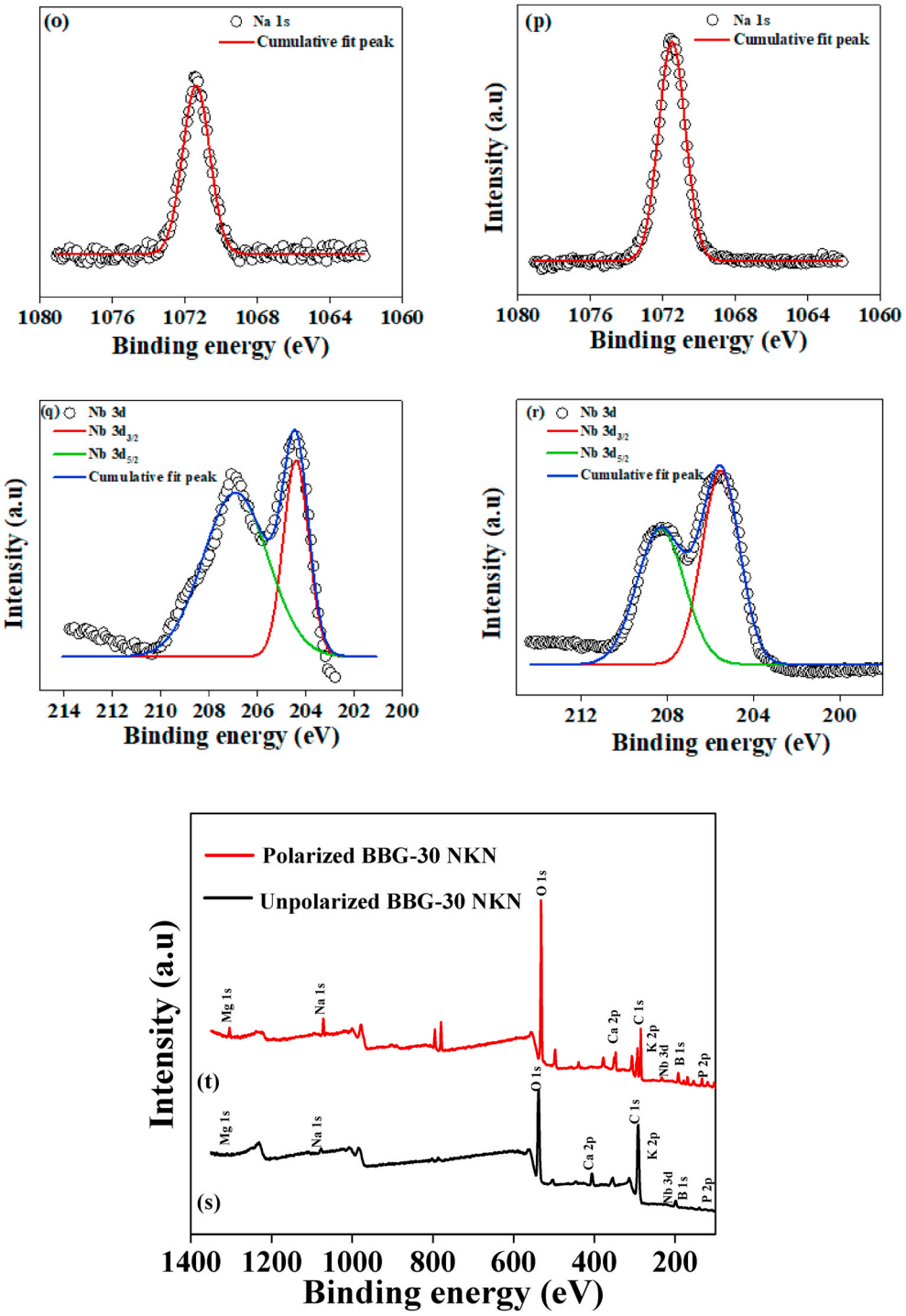

Fig. 5. (*continued*).

states i.e., (Ca $2p_{1/2}$–349.53 eV) and (Ca $2p_{3/2b}$–347.6 eV) [Fig. 4 (g, h)] [43]. The separation between the binding energies of Ca $2p_{1/2}$ and $Ca2p_{3/2}$ was ~3.5 eV. The Ca $2p_{3/2}$ spectra represent the presence of Ca^{2+} ions in the prepared composition [44]. The binding energies of C, associated with O – C = O and *C*–C, were measured to be ~ (284.0–285.2 eV) for both, unpolarized and polarized BBG samples [45]. The binding energies for O 1s (~530 eV), Mg 1s (~1304 eV) and Na 1s (~1073.93 eV) was measured for both, unpolarized and polarized BBG samples [46–48]. It was observed that the binding energies of associated elements in BBG were unaffected after polarization. The Ca/P ratio of unpolarized and polarized BBG was calculated using Casa XPS software and found to be ~1.81 and 1.62, respectively. The XPS analyses confirm that surface chemistry of prepared BBG samples were remain unaffected after polarization treatment. Fig. 5 represents the XPS spectra for unpolarized and polarized BBG-30 vol % NKN composite samples. It has been noticed that the binding energies of BBG elements (in BBG-30 vol % NKN composites) such as Mg, C, Ca, Na, O, P, B and K were similar as observed in pure BBG samples [Fig. 5 (a-p)]. The Nb 3d spectra were deconvoluted into two states i.e., Nb 3d $_{3/2}$ and Nb 3d $_{5/2}$ with binding energies of ~207.47 eV and 204.67 eV [Fig. 5 (q, r)], respectively, for both, unpolarized and polarized samples [49]. The Ca/P ratio for BBG-NKN (30 vol %) composites were calculated to be ~1.79 and 1.59

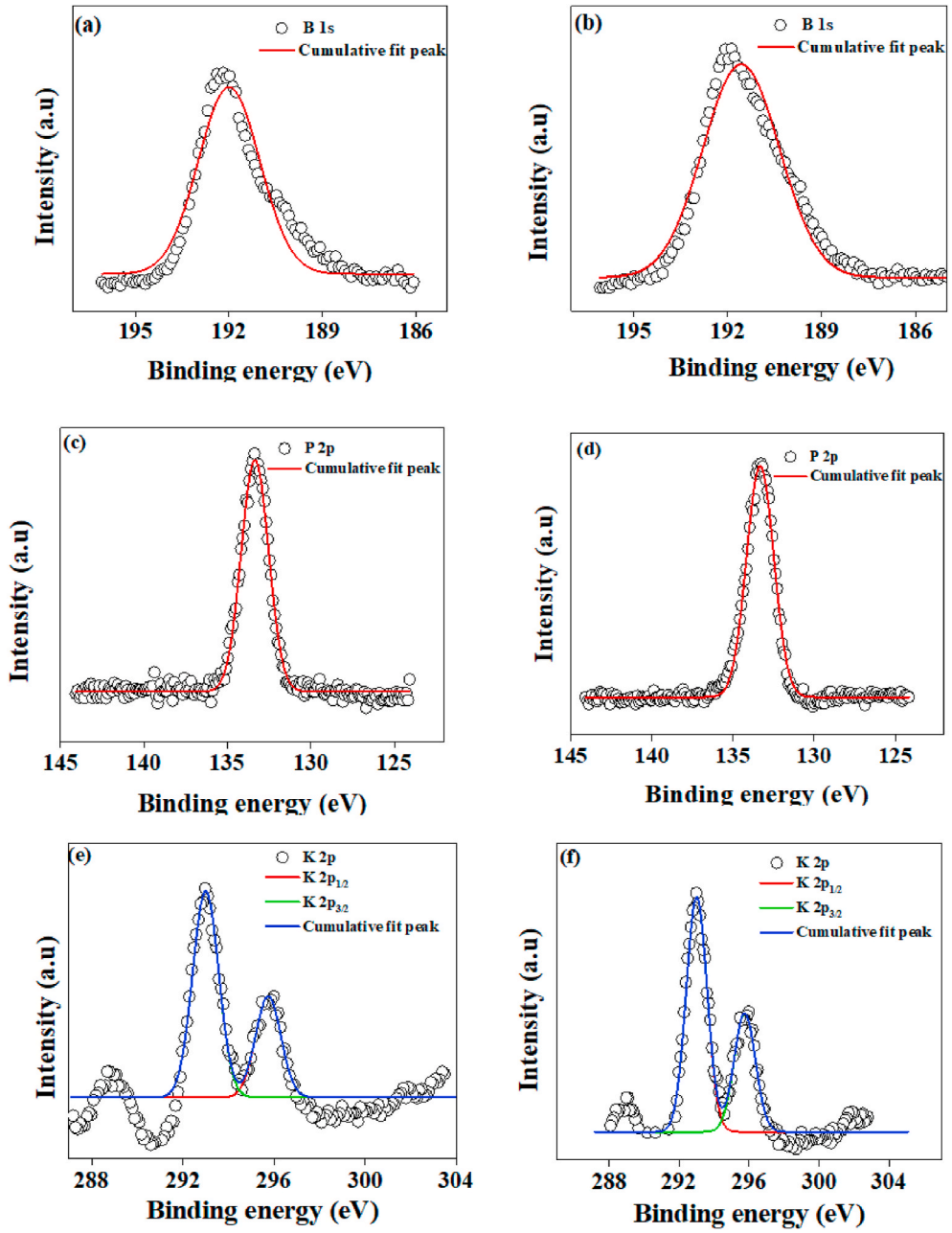

Fig. 6. The obtained and Gaussian fitted XPS spectra for unpolarized and polarized BBG- 30 vol% BT composites, (a, b) B 1s spectra, (c, d) P 2p spectra, (e, f), K 2p, (g, h) Ca 2p, (i, j) C, (k, l) O 1s, (m, n) Mg 1s, (o, p) Na 1s, (q, r) Ti 2p, (s, t) Ba 3d spectra and (u, v) represent the combination of all obtained XPS spectra for unpolarized and polarized BBG, respectively.

for unpolarized and polarized samples, respectively. The XPS spectra of BBG-30 vol % BT composite samples are represented as Fig. 6. The peaks of Mg, C, Ca, Na, O, P, B and K elements have similar binding energies as observed in BBG and BBG-3- vol. % NKN composite for both, unpolarized and polarized samples [Fig. 6 (a-p)]. The XPS spectra of BBG -30 vol % BT was fitted using Gaussian function and found that the Peaks of Ti^{4+} in $BaTiO_3$ possess two states i.e., Ti 2p $_{3/2}$ and Ti $2p_{1/2}$ with binding energies of ~457.7 and 463.4 eV, [Fig. 6 (q, r)], respectively [50]. Similarly, the peaks of Ba were splitted into two peaks i.e., Ba 3d $_{3/2}$ (~794.2 e V) and Ba 3d $_{5/2}$ (~779.4 eV) [Fig. 6 (s, t)] for both, unpolarized and polarized samples [51]. The binding energies of Ba 3d $_{3/2}$ and Ba 3d $_{5/2}$ were separated by ~1.5 eV [52]. The binding energy, corresponding to Ba 3d $_{5/2}$ spectrum confirms the perovskite phase of Ba in BT samples [53]. The Ca/P ratio for unpolarized and polarized BBG-30 vol % BT composites was calculated to be ~1.8 and 1.58, respectively. The XPS analyses for BBG and BBG-30 vol % NKN/BT composites suggest that surface polarization does not affect the surface chemistry of processed composite samples.

3.3. *In-vitro antibacterial response*

3.3.1. *MTT assay*

The quantitative analyses of *E. coli* and *S. aureus* bacteria, cultured on BBG and BBG-x NKN/BT (x = 30 vol %) composites are represented in Fig. 7 The viability of *E. coli* bacteria significantly reduces on developed BBG and BBG-NKN/BT composite samples as compared to control sample [correspond to (*) in Fig. 7 (a)]. However, for *S. aureus* bacteria, the unpolarized and polarized BBG and BBG-30 vol % NKN/BT

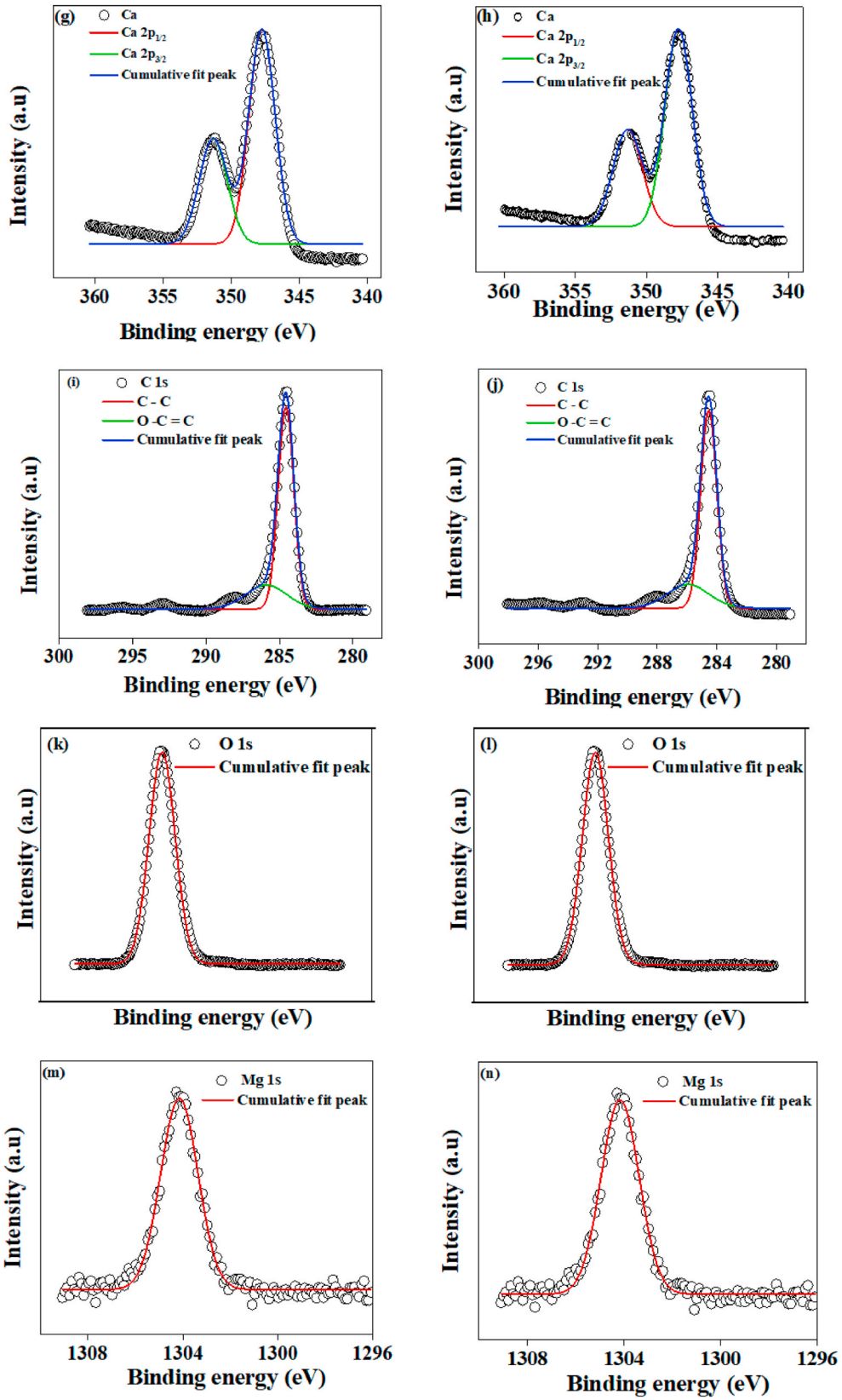

Fig. 6. (*continued*).

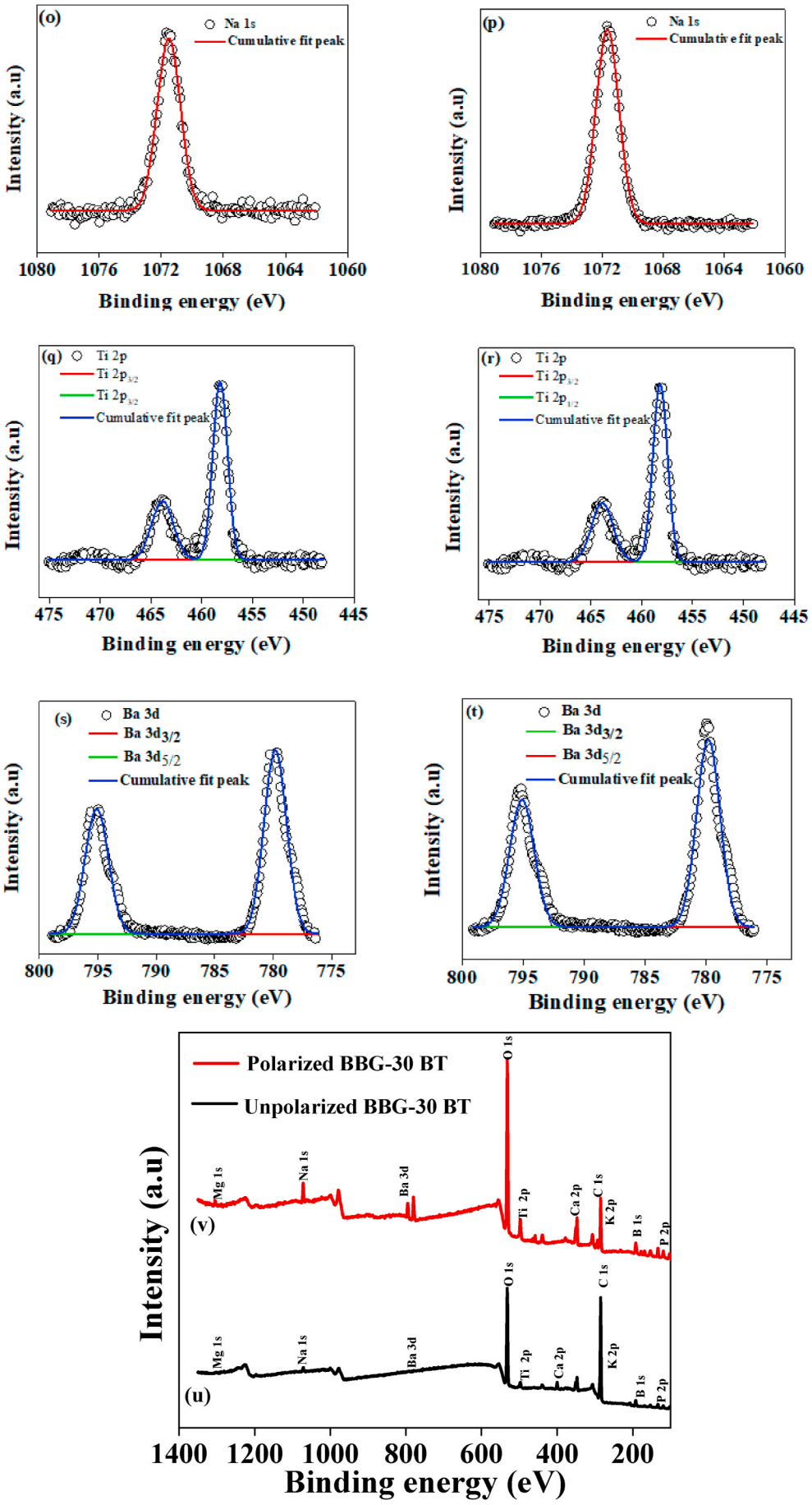

Fig. 6. (*continued*).

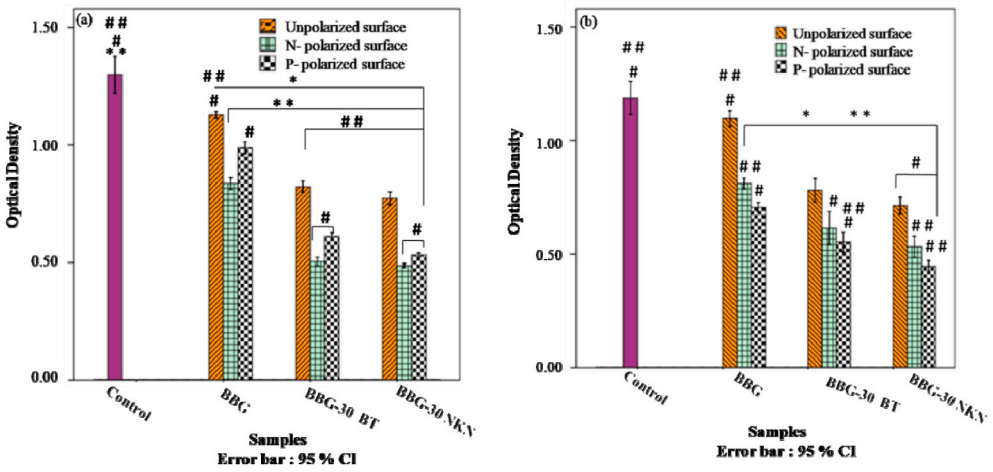

Fig. 7. The antibacterial response (MTT assay) of (a) *E. coli* and (b) *S. aureus* bacteria, cultured on unpolarized and polarized BBG-x NKN/BT (x = 30 vol %) samples. The symbols (*) and (**) represent the statistically significant difference among all the samples with respect to control sample (glass cover slip) and unpolarized BBG, respectively, at $p < 0.05$. The symbols (#) and (##) represent the statistically significant difference among all the samples with respect to N- polarized and P-polarized BBG, respectively, at $p \leq 0.05$.

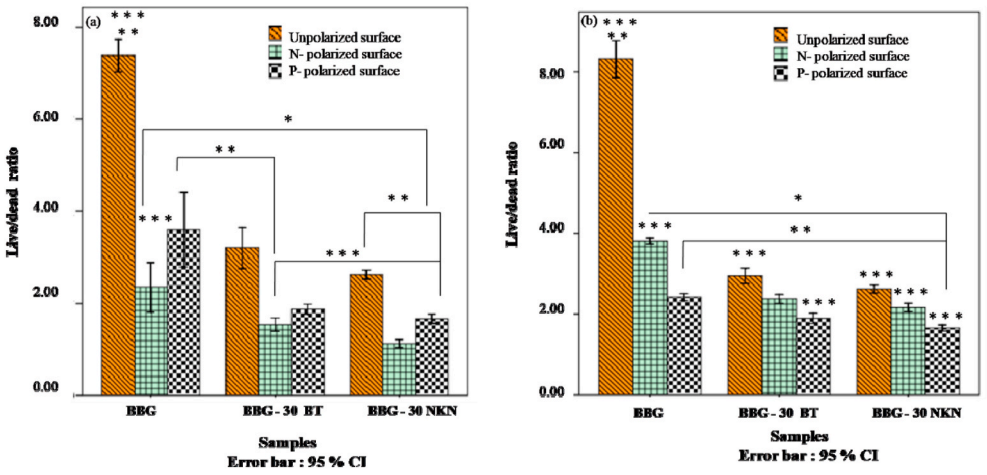

Fig. 8. Live/dead ratio for (a) *E. coli* and (b) *S. aureus* bacteria, while cultured on unpolarized and polarized BBG-x NKN/BT (x = 30 vol %) composites. The symbol (*) represents the statistically significant difference among all the samples with respect to unpolarized BBG, at $p \leq 0.05$. The symbols (**) and (***) represent the statistically significant difference among all the samples with respect to N- polarized and P-polarized BBG, respectively, at $p \leq 0.05$.

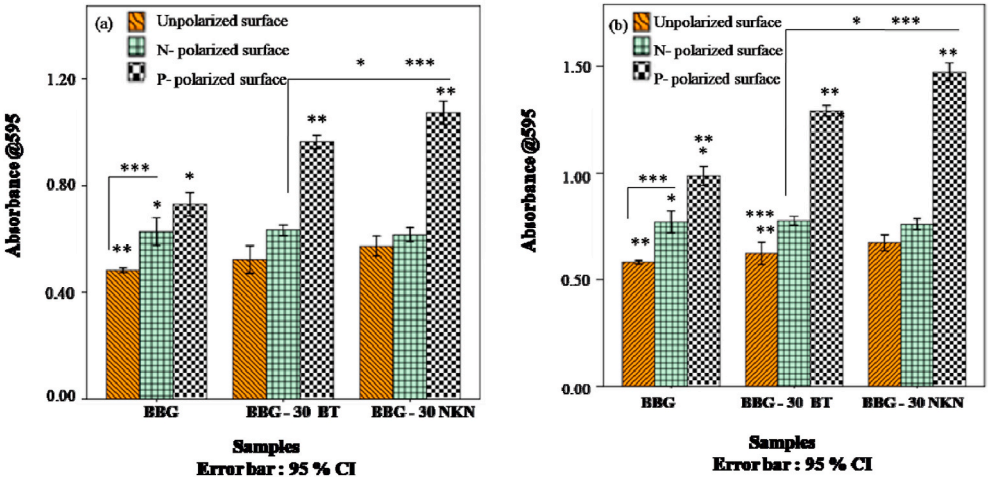

Fig. 9. Super oxide generation on unpolarized and polarized surfaces of BBG-x BT/NKN (x = 30 vol %) composites, while cultured with (a) *E. coli* and (b) *S. aureus* bacteria. The symbol (*) represents the statistically significant difference among all the samples with respect to unpolarized BBG at $p \leq 0.05$. The symbols (**) and (***) represent the statistically significant difference among all the samples with respect to N- polarized and P-polarized BBG, respectively, at $p \leq 0.05$.

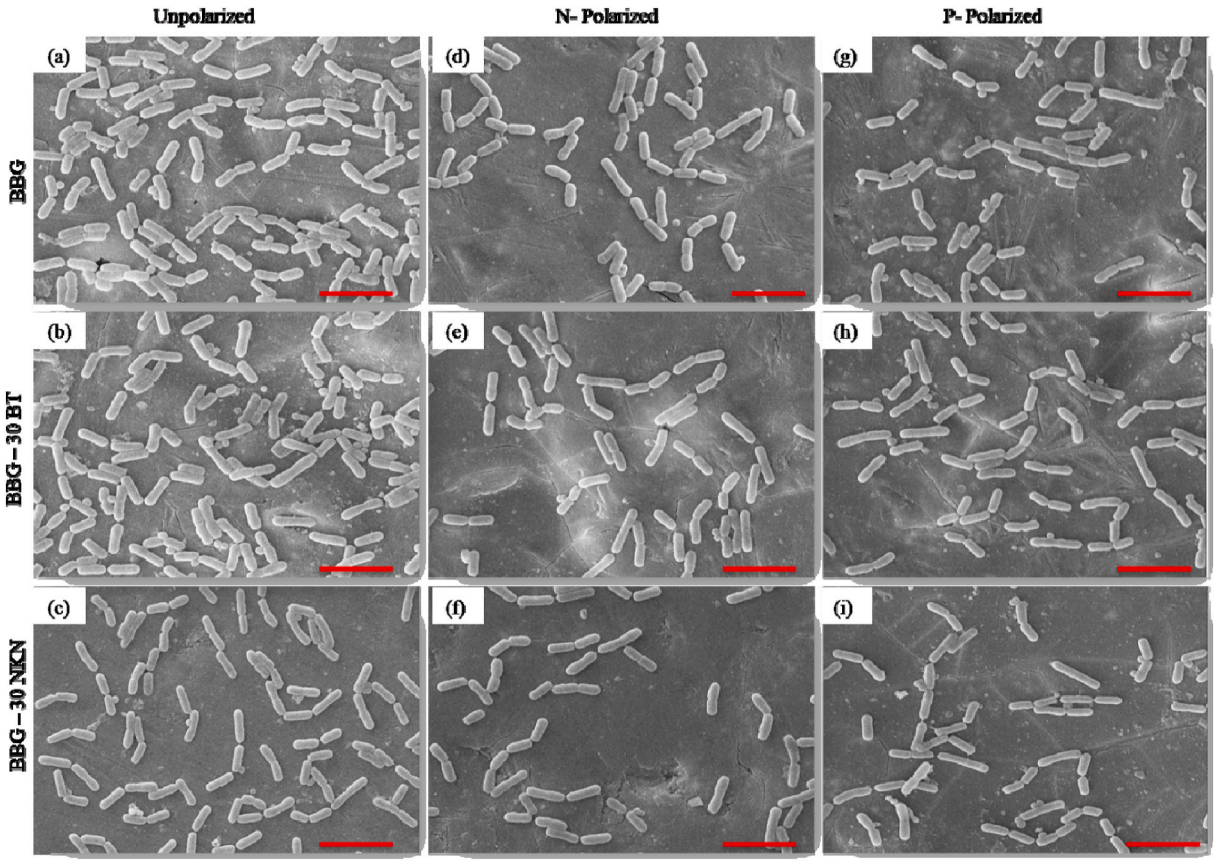

Fig. 10. The scanning electron microscopic images, demonstrating the adhesion of *E. coli* bacteria on unpolarized and polarized BBG-x BT/NKN (x = 30 vol %) composite sample surfaces (scale bar corresponds to 2 μm).

composites demonstrate significant reduction in viability [represented as (*) in Fig. 7 (b)]. The incorporation of NKN/BT as secondary phases enhances the antibacterial response of the prepared composite. The optical density, measured for both, *E. coli* and *S. aureus* bacteria significantly reduced on unpolarized and polarized BBG, BBG-30 NKN/BT composites, while compared with unpolarized BBG [represented as (**) in Fig. 7]. In addition, the surface polarization also affects the antibacterial response of BBG and its composites. The negatively polarized surfaces of BBG, BBG-30 NKN/BT composites illustrate significant reduction in optical density of *E. coli* bacteria. In case of *S. aureus* bacteria, positively polarized surfaces of BBG, BBG-30 NKN/BT composites demonstrate significant reduction in optical density. It is clearly observed that the optical density of *E. coli* bacteria significantly reduces on polarized BBG-30 NKN/BT samples [represented as (#) in Fig. 7 (a)] as compared to negatively polarized BBG. However, for *S. aureus* bacteria, the developed samples show significant difference in optical density, except BBG-30 BT [represented as (#) in Fig. 7 (b)], as compared to negatively polarized BBG. In contrast, optical density of *E. coli* bacteria reduces significantly on unpolarized and polarized BBG-30 BT/NKN composites [represented as (##) in Fig. 7 (b)] as compared to positively polarized BBG. However, for *S. aureus* bacteria, the optical density reduces significantly on polarized BBG-30 NKN/BT composites [represented as (##) in Fig. 7 (b)]. Although, MTT results demonstrate that addition of NKN and BT as secondary phases as well as polarization increases the antibacterial behavior of BBG and their composites. NKN incorporation in BBG matrix, on the other hand, has a better antibacterial response than BT.

3.3.2. *Live/dead ratio*

Fig. 8 represents the live/dead ratio for *E. coli* and *S. aureus* bacteria, cultured on BBG-x NKN/BT (x = 30 vol %) composite samples. The incorporation of piezoelectric NKN/BT as secondary phase in BBG reduces the live/dead ratio for BBG-30 NKN/BT composites. The statistical analyses demonstrate that live/dead ratio for both, *E. coli* and *S. aureus* bacteria significantly decreases on unpolarized and polarized BBG-30 NKN/BT composites as compared to unpolarized BBG [represented as (*) in Fig. (8)]. The polarized surfaces also demonstrate bacteria specific antibacterial response. The live/dead ratio for *E. coli* bacteria significantly reduced on negatively polarized surfaces. However, positively polarized surfaces demonstrate significant reduction in live/dead ratio for *S. aureus* bacteria. It is observed that negatively polarized BBG- 30 NKN sample demonstrates minimum (~1.58) live/dead ratio for *E. coli* bacteria. However, positively polarized BBG- 30 NKN sample has minimum (~1.82) live/dead ratio for *S. aureus* bacteria. Overall, the addition of piezoelectric NKN/BT as secondary phase as well as polarization induced surface charge reduces the live/dead ratio for both, *E. coli* and *S. aureus* bacteria.

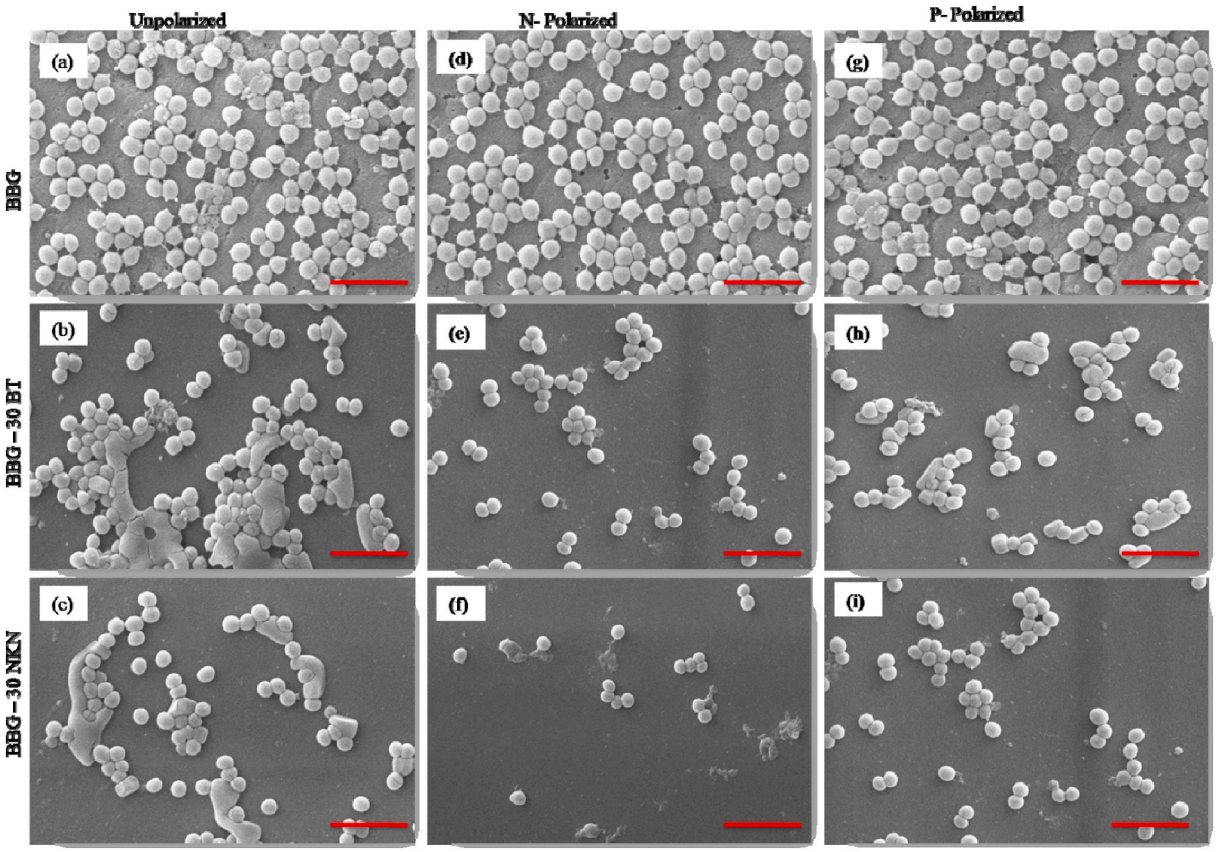

Fig. 11. The scanning electron microscopic images, demonstrating the adhesion of *S. aureus* bacteria on unpolarized and polarized BBG-x BT/NKN (x = 30 vol %) composite sample surfaces (scale bar corresponds to 2 μm).

3.3.3. Nitro blue tetrazolium (NBT) assay

Fig. 9 represents the superoxide ions, produced on BBG-x BT/NKN (x = 30 vol %) composite samples, while cultured with *E. coli* and *S. aureus* bacteria. The positively charged surfaces reveal higher superoxide production as compared to negatively polarized and unpolarized surfaces. The statistical analyses suggest that incorporation of NKN (30 vol %) piezoelectric in BBG matrix enhances the superoxide production significantly on unpolarized samples for both the bacteria. However, in BBG-BT composite, the superoxide production for both the bacteria significantly increased on polarized surfaces only. The superoxide production for *E. coli* bacteria increased by about 48.32, 72.40 and 113.43% on positively charged BBG, BBG-30 BT and BBG-30 NKN composite samples, respectively, while compared with unpolarized BBG. Similarly, for *S. aureus* bacteria, superoxide production was increased by about 72.45, 131.35, and 150.47% on positively charged BBG, BBG-30 BT and BBG-30 NKN composite samples respectively, while compared with unpolarized BBG. It is observed that positively polarized surfaces are more prominent for generation of superoxide ions [54]. The polarized surfaces generate micro-electric field which promote the ROS generation [55]. The produced ROS can damage the outer structure of bacterial cells as well as DNA and proteins. The electric field, generated by polarization, disrupts the Fe– S clusters [56]. The damage of Fe– S clusters produce H_2O_2 through Fenton reaction (Eqs. (4) and (5)) which can injure the DNA of bacterial cells [57].

$$O_2^- + Fe^{3+} \rightarrow O_2 + Fe^{2+} \quad (4)$$

$$H_2O_2 + Fe^{2+} \rightarrow OH^{\cdot} + OH^- + Fe^{2+} \quad (5)$$

Overall, it has been observed that positively charged surfaces can produce higher amount of superoxide as compared to unpolarized surfaces.

3.3.4. Bacterial adhesion test

Fig. 10 represents the scanning electron microscopic images of *E. coli* bacteria, adhered on BBG-x BT/NKN (x = 30 vol %) composite samples. It is clearly noticed that the incorporation of NKN/BT in BBG reduces the adhesion of *E. coli* bacteria [Fig. 10 (a-i)]. Regardless of secondary phase addition, polarized surfaces also reduce the bacterial adhesion. The negatively charged surfaces of all the developed samples demonstrate lower adhesion of *E. coli* bacteria as compared to unpolarized and positively polarized surfaces [Fig. 10 (d-f)]. However, positively polarized surfaces demonstrate lower bacterial adhesion as compared to unpolarized BBG [Fig. 10 (g-i)]. The interaction between negatively charged surface and *E. coli* bacteria (negatively charged) is responsible for lower adhesion of *E. coli* bacteria on negatively charged surfaces [35]. The microscopic images of *E. coli* bacteria, adhered on BBG-x BT/NKN composite support the MTT assay results.

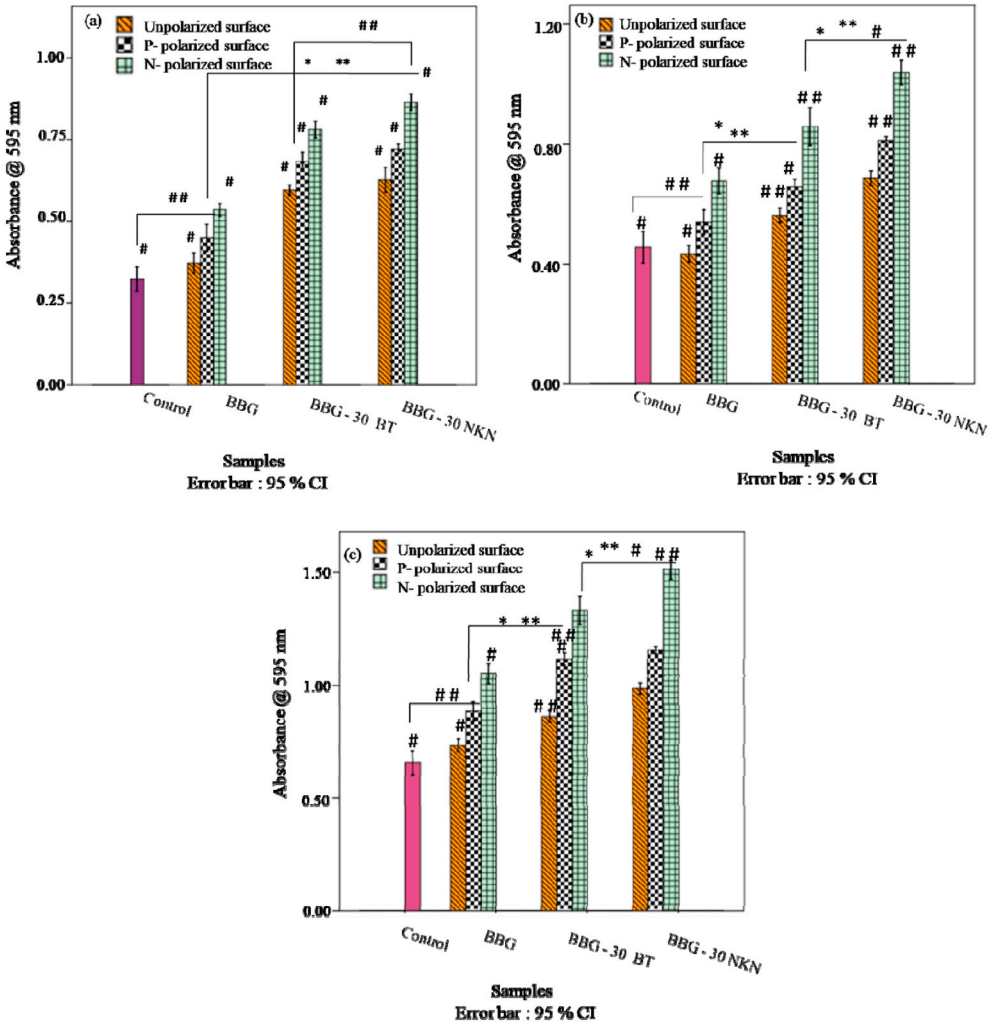

Fig. 12. The viability of osteoblast-like MG-63 cells, cultured on BBG, and BBG – x BT/NKN (x = 30 vol %) composites after incubation for (a) 3 (b) 5 and (c) 7 days. The symbols (*) and (**) represent the statistically significant difference among all the samples with respect to control sample (glass cover slip) and unpolarized BBG, respectively, at $p \leq 0.05$. The symbols (#) and (##) represent the statistically significant difference among all the samples with respect to P-polarized and N- polarized BBG, respectively, at $p \leq 0.05$.

Fig. 11 represents the SEM micrographs of *S. aureus* bacteria, adhered on BBG-x BT/NKN (x = 30 vol %) composite samples. The adhesion of *S. aureus* bacteria depends upon addition of piezoelectric NKN/BT as secondary phase in BBG matrix. It is clearly observed that unpolarized surfaces of BBG-30 vol % BT and BBG-30 vol % NKN composite samples demonstrate lower adhesion of *S. aureus* bacteria, as compared to unpolarized BBG sample surface [Fig. 11 (a-c)]. In addition, the polarized surfaces of all the compositions reduce the bacterial adhesion as compared to unpolarized BBG sample.

The above-mentioned results confirm that the addition of piezoelectric BT and NKN as the secondary phases in BBG matrix enhances the antibacterial behavior. However, it has been reported that BBG itself exhibits antibacterial nature due to the presence of network modifier elements such as K, Mg [58,59]. It has been demonstrated that these network modifiers have the tendency to dissolve in the culture solution which alter the pH of the solution [60].

It has been demonstrated that the presence of borate (B_2O_3) in BBG can reduce the bacterial infection [61]. In addition, piezoelectric BT and NKN are known to be antibacterial and biocompatible materials [62]. The prepared composite releases sodium and potassium molecules or ions in the bacterial extracellular matrix due to presence of NKN secondary phase. It has been suggested that these ions exhibit the physiochemical characteristics which are unfavorable for bacterial growth. For example, potassium is hygroscopic in nature which soaks the intracellular water when interact with bacterial cell wall and consequently, inhibit the bacterial growth [29,63,64]. Apart from incorporation of piezoelectric secondary phases, polarization induced surface charges are also responsible for such antibacterial response [65]. Outer membranes of the gram-negative and gram-positive bacterial cells possess negative charge [66]. The surface charge induced by the polarization interact with cell membrane and repel the gram-negative bacteria due to more negative charge as compared to gram positive bacterial cells [67]. On the other hand, positively charged surface neutralizes the negative charge of bacteria and alter the architecture of lipid layer by enhancing the permeability of cell membrane which consequently, damages the bacterial cells and lead to cell death [68–70]. The hydrophilicity of polarized surface can also be an influential factor for such type of antibacterial behavior [71]. It has been reported that polarization increases the hydrophilicity of surfaces and such surfaces resist the bacterial adhesion [72].

3.4. In-vitro cytocompatibility

3.4.1. MTT assay

Fig. 12 represents the viability of MG-63 cells in terms of optical density, after 3, 5 and 7 days of incubation. The viability of MG-63 cells increases with addition of piezoelectric phase in BBG matrix.

The polarization of the developed sample surfaces also favors the proliferation of MG-63 cells after incubation of up to 7 days. The optical densities of all the samples, expect unpolarized BBG, demonstrate significant enhancement as compared to control sample, after incubation of 3, 5, and 7 days [correspond to (*) in Fig. (12)]. In addition, the negatively charged surfaces of all the compositions illustrate higher proliferation of MG-63 cells as compared to unpolarized and positively

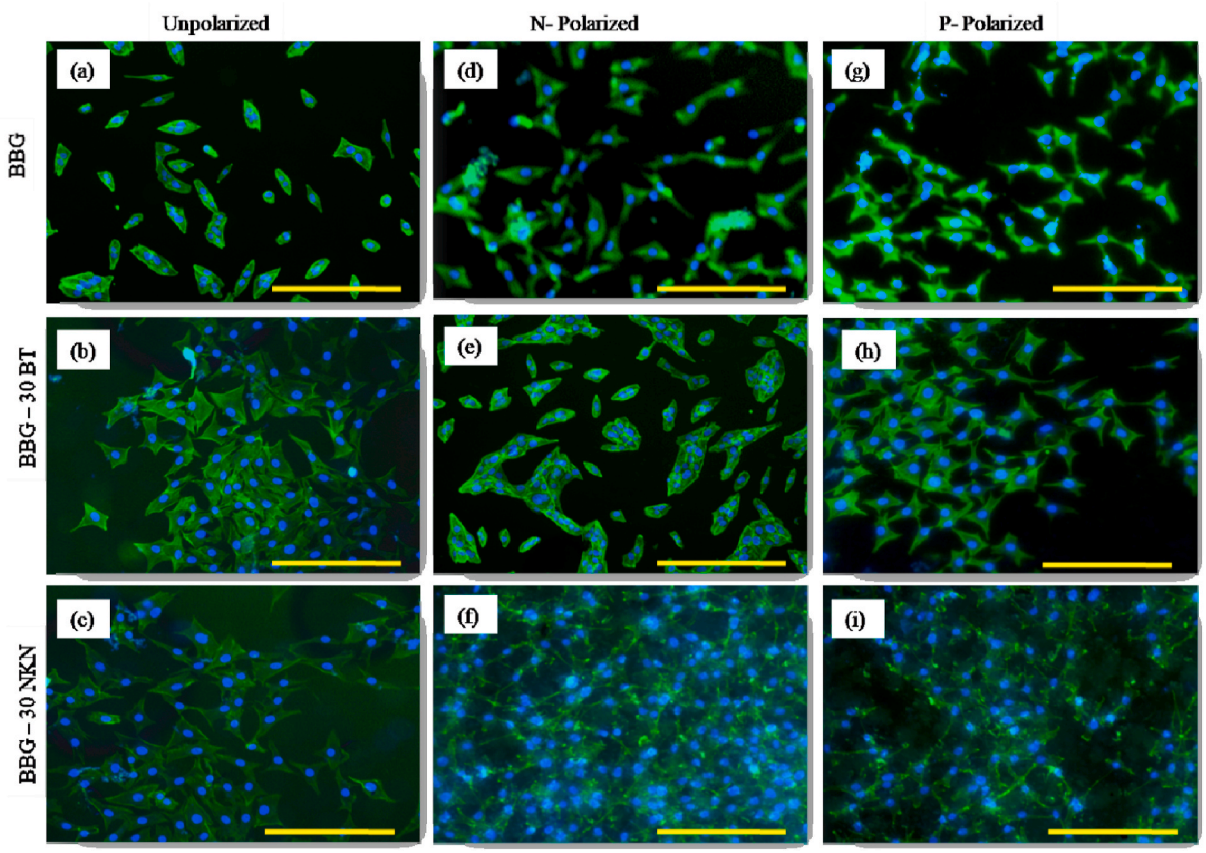

Fig. 13. Fluorescence images of MG-63 cells, adhered on unpolarized and polarized surfaces of BBG-x BT/NKN (x = 30 vol %) composite samples, after incubation of 3 days (scale bars corresponds to 100 μm).

polarized sample surfaces of respective composition and culture periods. The viability of MG-63 cells on negatively polarized BBG, BBG-BT (30 vol %) and BBG-NKN (30 vol %) composites are calculated to be about (43, 109, 131%), (81, 130, 178%) and (181, 252, 304%), after 3, 5, and 7 days of incubation respectively, as compared to unpolarized BBG sample. Overall, it is observed that viability of MG-63 cells increases with incubation period, addition of BT/NKN as secondary phases as well as polarization induced surface charge.

3.4.2. *Cell morphology*

The adhesion of MG-63 cells on BBG-x (x = 30 vol %) BT/NKN composite was observed using fluorescence microscopic images. Fig. 13 represents the adhered MG-63 cells on BBG-x BT/NKN (x = 30 vol %) composite samples, after 3 days of culture. The density of MG-63 cells increases with incorporation of piezoelectric NKN/BT (30 vol %) on composite sample surfaces as compared to unpolarized BBG [Fig. 13 (a-c)]. Irrespective of addition of secondary phases, the polarized surfaces also enhance the cell density. The negatively polarized surfaces have higher cell density while compared with unpolarized and positively polarized surfaces of the same sample [Fig. 13 (d-f)]. The density of adhered MG-63 cells is observed to be maximum on BBG-30 vol % NKN composite samples [Fig. 13 (f)]. Overall, the negatively polarized surfaces have higher cell density in comparison to unpolarized and positively polarized surfaces.

It has been reported that BBG releases K^+, Na^+, BO_3^{3-} and PO_4^{3-} ions after immersion in physiological solution. The presence of Ca^{2+} ions in the media react with released BO_3^{3-} and PO_4^{3-} ions and start the formation of hydroxyapatite layer [73,74]. In addition, released ions promote the osteogenic gene expression [75]. It has been observed that the proliferation of MG-63 cells increases with incorporation of piezoelectric BT/NKN in BBG. Apart from addition of piezoelectric secondary phases, the polarized substrates also increase the cell viability.

The negatively charged NKN and BT surfaces attract Ca^{2+} ions, present in the media and these ions react with the charged proteins, available in the cell medium and support the adhesion of MG-63 cells [76]. The negatively charged surfaces of HA-30 vol % BT, and HA-30 vol % NKN composites demonstrate higher adhesion and proliferation of MG-63 cells [27,77].

4. Conclusions

The BBG was successfully synthesized using melt quench method and BBG-NKN (30 vol %) and BBG -BT (30 vol %) composites were prepared using solid state mixing route. The XRD analyses confirm the formation of pure phase BBG. The distinct phases of BT and NKN were observed in composite samples. The BBG demonstrates inherent antibacterial property due to presence of boron. The incorporation of piezoelectric BT/NKN (30 vol %) in BBG enhances the antibacterial response. The adhesion of *E. coli* and *S. aureus* bacteria on negatively polarized surfaces has been reduced due to electrostatic repulsion between charge on bacterial membrane (negative charge) and material surface. On the other hand, negatively charged surfaces promote the proliferation and adhesion of MG-63 cells. Overall, it can be concluded that the addition of piezoelectric BT/NKN (30 vol %) in BBG and polarization increases the

antibacterial activity as well as cell proliferation.

Conflicts of interest

This is to confirm that there is no conflict of interest to declare.

Acknowledgements

The financial support from SERB, DST, Govt. of India is gratefully acknowledged.

References

[1] M. Vallet-Regí, Evolution of bioceramics within the field of biomaterials, C. R. Chim. 13 (2010) 174–185, https://doi.org/10.1016/j.crci.2009.03.004.
[2] L.L. Hench, R.J. Splinter, W.C. Allen, T.K. Greenlee, Bonding mechanisms at the interface of ceramic prosthetic materials, J. Biomed. Mater. Res. Symp. 2 (1971) 117–141, https://doi.org/10.1002/jbm.820050611.
[3] A.S. Verma, A. Singh, D. Kumar, A.K. Dubey, Electro-mechanical and polarization-induced antibacterial response of 45S5 bioglass–sodium potassium niobate piezoelectric ceramic composites, ACS Biomater. Sci. Eng. 6 (5) (2020) 3055–3069, https://doi.org/10.1021/acsbiomaterials.0c00091.
[4] L.L. Hench, J.M. Polak, Third-generation biomedical materials, Science 295 (2002) 1014–1017, https://doi.org/10.1126/science.1067404.
[5] Q. Fu, M.N. Rahaman, B.S. Bal, L.F. Bonewald, K. Kuroki, R.F. Brown, Bioactive glass scaffolds for bone tissue engineering: state of the art and future perspectives, J. Biomed. Mater. Res. A 95 (2010), 172e179, https://doi.org/10.1016/j.msec.2011.04.022.
[6] Francesco Baino, Bioactive glasses – when glass science and technology meet regenerative medicine, Ceram. Int. 44 (2018) 14953–14966, https://doi.org/10.1016/j.ceramint.2018.05.180.
[7] M.N. Rahaman, D.E. Day, B.S. Bal, Q. Fu, S.B. Jung, L.F. Bonewald, A.P. Tomsia, Bioactive glass in tissue engineering, Acta Biomater. 7 (2011), 2355e2373, https://doi.org/10.1016/j.actbio.2011.03.016.
[8] D. Zhang, O. Lepparanta, E. Munukka, H. Ylanen, M. Viljanen, E. Eerola, M. Hupa, L. Hupa, Antibacterial effects and dissolution behavior of six bioactive glasses, J. Biomed. Mater. Res. 93 (2009) 475–483, https://doi.org/10.1002/jbm.a.32564.
[9] M. Hamadouche, A. Meunier, D.C. Greenspan, C. Blanchat, J.P. Zhong, G.P. L. Torre, L. Sedel, Long-term in vivo bioactivity and degradability of bulk sol–gel bioactive glasses, J. Biomed. Mater. Res. 54 (2001), https://doi.org/10.1002/1097-4636(20010315)54:4<560::AID-JBM130>3.0.CO;2-J, 560–6.
[10] D.E. Day, J.E. White, R.E. Brown, K.D. McMenamin, Transformation of borate glasses into biologically useful materials, Glass Technol. 44 (2003) 75–78.
[11] W. Huang, M.N. Rahaman, D.E. Day, Y. Li, Mechanisms for converting bioactive silicate, borate, and borosilicate glasses to hydroxyapatite in dilute phosphate solution, Phys. Chem. Glasses: Eur. J. Glass Sci. Technol. B47 (2006) 647–658.
[12] L. Bi, S. Jung, D. Day, K. Neidig, V. Dusevich, D. Eick, L. Bonewald, Evaluation of bone regeneration, angiogenesis, and hydroxyapatite conversion in critical-sized rat calvarial defects implanted with bioactive glass scaffolds, J. Biomed. Mater. Res. 100 (12) (2012) 3267–3275, https://doi.org/10.1002/jbm.a.34272. Dec.
[13] M.L. Cooper, J.F. Hansbrough, Use of a composite skin graft composed of cultured human keratinocytes and fibroblasts and a collagen-GAG matrix to cover full-thickness wounds on athymic mice, Feb, Surgery 109 (2) (1991) 198–207. PMID: 1992553.
[14] X. Qu, H. Yang, B. Jia, Z. Yu, Y. Zheng, K. Dai, Biodegradable Zn–Cu alloys show antibacterial activity against MRSA bone infection by inhibiting pathogen adhesion and biofilm formation, Acta Biomater. 117 (2020) 400–417, https://doi.org/10.1016/j.actbio.2020.09.041.
[15] A. Bordbar-Khiabani, B. Yarmand, M. Mozafari, Enhanced corrosion resistance and in-vitro biodegradation of plasma electrolytic oxidation coatings prepared on AZ91 Mg alloy using ZnO nanoparticles-incorporated electrolyte, Surf. Coating. Technol. 360 (2019) 153–171, https://doi.org/10.1016/j.surfcoat.2019.01.002.
[16] L. Tamayo, M. Azocar, M. Kogan, A. Kogan, Riveros, M. Paez, Copper-polymer nanocomposites: an excellent and cost-effective biocide for use on antibacterial surfaces, Mater. Sci. Eng. C 69 (2016) 1391–1409, https://doi.org/10.1016/j.msec.2016.08.041.
[17] M. Bellantone, H.D. Williams, L.L. Hench, Broad-spectrum bactericidal activity of Ag2O-doped bioactive glass, Antimicrob. Agents Chemother. 46 (2002) 1940–1945, https://doi.org/10.1128/AAC.46.6.1940-1945.2002.
[18] X. Niu, H. Shen, J. Fu, J. Feng, Effective control of microstructure evolution in AZ91D magnesium alloy by SiC nanoparticles in laser powder-bed fusion, Mater. Des. 206 (2021), 109787, https://doi.org/10.1016/j.matdes.2021.109787.
[19] L. Drago, M. Toscano, M. Bottagisio, Recent evidence on bioactive glass antimicrobial and antibiofilm activity: a mini-review, Materials 11 (2018) 1–11, https://doi.org/10.3390/ma11020326.
[20] N. Gupta, D. Santhiya, S. Murugavel, A. Kumar, A. Aditya, M. Ganguli, S. Gupta, Effects of transition metal ion dopants (Ag, Cu and Fe) on the structural, mechanical and antibacterial properties of bioactive glass, Colloids Surf., A 538 (2018) 393–403, https://doi.org/10.1016/j.colsurfa.2017.11.023.
[21] Q. Fu, M.N. Rahaman, H. Fu, X. Liu, Silicate, borosilicate, and borate bioactive glass scaffolds with controllable degradation rate for bone tissue engineering applications. I. Preparation and in vitro degradation, J. Biomed. Mater. Res. 95 (2010) 164–171, https://doi.org/10.1002/jbm.a.32824.
[22] Megan Ottomeyer, Ali Mohammadkah, Delbert Day, David Westenberg, Broad-spectrum antibacterial characteristics of four novel borate-based bioactive glasses" Adv. Microbiol., 6 (10), 201, DOI: 10.4236/aim.2016.610076..
[23] A D. Wang, W. Huang, Q. Fu, M.N. Rahaman, D.E. Day, In vitro bioactive characteristics of borate-based glasses with controllable degradation behavior, J. Am. Ceram. Soc. 90 (2007) 303–306, https://doi.org/10.1111/j.1551-2916.2006.01358.x.
[24] P. Balasubramanian, A. Grünewald, R. Detsch, L. Hupa, B. Jokic, F. Tallia, A. K. Solanki, J.R. Jones, A.R. Boccaccini, Ion release, hydroxyapatite conversion, and cytotoxicity of boron-containing bioactive glass scaffolds, Int. J. Appl. Glass Sci. 7 (2016) 206–215, https://doi.org/10.1111/ijag.12206.
[25] W. Chang, M. Colangeli, S. Colangeli, C. Di Bella, E. Gozzi, D. Donati, Adult osteomyelitis: debridement versus debridement plus Osteoset T pellets, Acta Orthop. Belg. 73 (2007) 238–243.
[26] S. Swain, R.N. Padhy, T.R. Rautray, Polarized piezoelectric bioceramic composites exhibit antibacterial activity, Mater. Chem. Phys. 239 (2020), 122002, https://doi.org/10.1016/j.matchemphys, 2019.
[27] A. Singh, A.K. Dubey, Improved antibacterial and cellular response of electrets and piezobioceramics, J. Biomater. Appl. (2021), 0885328221991965, https://doi.org/10.1177/0885328221991965.
[28] D. Khare, B. Basu, A. Dubey, K. Dubey, Electrical stimulation and piezoelectric biomaterials for bone tissue engineering applications, Biomaterials 258 (2020), 120280, https://doi.org/10.1016/j.biomaterials.2020.120280. ISSN 0142-9612.
[29] D. Khare, A. Singh, A.K. Dubey, Influence of Na and K contents on the antibacterial response of piezoelectric biocompatible NaxK1-xNbO3 (x = 0.2–0.8), Mater. Today Commun. 27 (2021), 102317, https://doi.org/10.1016/j.mtcomm.2021.102317. ISSN 2352-4928.
[30] A.S. Verma, D. Kumar, A.K. Dubey, Antibacterial and cellular response of piezoelectric Na0. 5K0. 5NbO3modified 1393 bioactive glass, Mater. Sci. Eng. C 116 (2020), 11138, https://doi.org/10.1016/j.msec.2020.111138.
[31] Y.B. Liu, D.A. Peterson, H. Kimura, D. Schubert, Mechanism of cellular 3–(4,5-dimethylthiazol-2-yl)-2,5- diphenyltetrazolium bromide (MTT) reduction, J. Neurochem. 69 (1997) 581–593, https://doi.org/10.1046/j.1471-4159.1997.69020581.x.
[32] G. Thrivikramana, P.K. Mallik, B. Basu, Substrate conductivity dependent modulation of cell proliferation and differentiation, In -Vitro. Biomaterials 34 (2013) 7073–7085, https://doi.org/10.1016/j.biomaterials.2013.05.076.
[33] H.S. Choi, J.W. Kim, Y.N. Cha, C. Kim, A quantitative nitrobluetetrazolium assay for determining intracellular superoxide anion production in phagocytic cells, J. Immunoassay Immunochem. 27 (2006) 31–44, https://doi.org/10.1080/15321810500403722.
[34] M.V. Berridge, P.M. Herst, A.S. Tan, Tetrazolium dyes as tools in cell biology: new insights into their cellular reduction Biotech, Annual Reviews 11 (2005) 127–152, https://doi.org/10.1016/S1387-2656(05)11004-7.
[35] Z. Huang, J. Chen, X. Li, H. Liu, J. Li, T. Ren, Y. Yang, S. Zhong, Polymethacrylic acid encapsulated TiO_2 nanotubes for sustained drug release and enhanced antibacterial activities, New J. Chem. 43 (2019) 1827–1837, https://doi.org/10.1039/C8NJ04568B.
[36] A. Singh, K. Reshma, A.K. Dubey, Combined effect of surface polarization and ZnO addition on antibacterial and cellular response of Hydroxyapatite-ZnO composites, Mater. Sci. Eng. C 107 (2020), 110363, https://doi.org/10.1016/j.msec.2019.110363. ISSN 0928-4931.
[37] J. Fayos, R.A. Howie, F.P. Glasser, Structure of calcium sodium pentaborate, Acta Crystallogr. Sect. C Cryst. Struct. Commun. 41 (10) (1985) 1394–1396, https://doi.org/10.1107/S0108270185007909.
[38] M.D.C.B. Lopez, G. Fourlaris, B. Rand, F.L. Riley, Characterization of barium titanate powders: barium carbonate identification, J. Am. Ceram. Soc. 82 (1999) 1777–1786, https://doi.org/10.1111/j.1151-2916.1999.tb01999.x.
[39] A. Polotai, A.V. Ragulya, T.V. Tomila, C.A. Randall, The XRD and IR study of the barium titanatenano-powder obtained via oxalate route, Ferroelectrics 298 (2004) 243–251, https://doi.org/10.1080/00150190490423624.
[40] S. Roth, F. Matsui, T. Greber, J. Osterwalder, Chemical vapor deposition and characterization of aligned and incommensurate graphene/hexagonal boron nitride heterostack on Cu(111), Nano Lett. 13 (2013) 2668–2675, https://doi.org/10.1021/nl400815w.
[41] H. Lu, T. Zhang, X. Wang, Q. Fang, Mater J., Sci.: Mater. Med. 20 (2009) 793.
[42] B. Zhou, Z. Sun, Y. Yao, Y. Pan, Phys. Chem. Miner. 39 (2012) 363.
[43] B. Zhou, Z. Sun, Y. Yao, Pan Phys. Chem. Miner. 39 (2012) 363.
[44] Y. Li, C. Zhao, H. Chen, C. Liang, L. Duan, W. Zhou, Modified CaO-based sorbent looping cycle for CO2 mitigation, Fuel 88 (2009) 697–704, https://doi.org/10.1016/j.fuel.2008.09.018.
[45] G. Greczynski, L. Hultman, C 1s peak of adventitious carbon aligns to the vacuum level: dire consequences for material's bonding assignment by photoelectron spectroscopy, ChemPhysChem 18 (2017) 1507–1512.
[46] P. Li, X. Zhao, C.J. Jia, H. Sun, L. Sun, X. Cheng, L. Liu, W. Fan, ZnWO4/BiOI heterostructures with highly efficient visible light photocatalytic activity: the case of interface lattice and energy level match, J. Mater. Chem. A 1 (2013) 3421–3429, https://doi.org/10.1039/C3TA00442B.
[47] Y. Gao, Y. Zhang, P. Chen, Y. Li, M. Liu, T. Gao, D. Ma, Y. Chen, Z. Cheng, X. Qiu, W. Duan, Z. Liu, Toward single-layer uniform hexagonal boron nitride–graphene patchworks with zigzag linking edges, Nano Lett. 13 (2013) 3439–3443, https://doi.org/10.1021/nl4021123.
[48] N. Guo, J. Wei, L. Fan, Y. Jia, D. Liang, H. Zhu, K. Wang, D. Wu, Controllable growth of triangular hexagonal boron nitride domains on copper foils by an

improved low-pressure chemical vapor deposition method, Nanotechnology 23 (1–6) (2012), 415605, https://doi.org/10.1088/0957-4484/23/41/415605.
[49] R. Fontaine, R. Caillat, L. Feve, M.J. Guittet, J. Electron. Spectrosc. Relat. Phenom. 10 (1977) 349, https://doi.org/10.1166/jnn.2009.1087.
[50] S.M. Mukhopadhyay, Tim C.S. Chen, J. Mater. Res. 10 (1995) 1502, https://doi.org/10.1557/JMR.1995.1502.
[51] M.C. Lopez, B.G. Fourlaris, B. Rand, L. Riley, J. Am. Ceram. Soc. 82 (1999) 1777, https://doi.org/10.1111/j.1151-2916.1999.tb01999.x.
[52] Y. Fujisaki, Y. Shimamoto, Matsui Jpn. J. Appl. Phys. 38 (1999) L52. Part 2.
[53] C. Miot, E. Husson, C. Proust, R. Erre, J.P. Coutures, J. Mater. Res. 12 (1997) 2388, https://doi.org/10.1557/JMR.1997.0316.
[54] J.M. Slauch, How does the oxidative burst of macrophages kill bacteria Still an open question, Mol. Microbiol. 80 (3) (2011) 580–583, https://doi.org/10.1111/j.1365-2958.2011.07612.x.
[55] G. Applerot, A. Lipovsky, R. Dror, N. Perkas, Y. Nitzan, R. Lubart, A. Gedanken, Enhanced antibacterial activity of nanocrystalline ZnO due to increased ROS-mediated cell injury, Adv. Funct. Mater. 19 (2009) 842–852, https://doi.org/10.1002/adfm.200801081.
[56] A.T. Poortinga, J. Smit, H.C. Van der Mei, J.H. Busscher, Electric field induced desorption of bacteria from a conditioning film covered substratum, Biotechnol. Bioeng. 76 (2001) 395–399, https://doi.org/10.1002/bit.10129.
[57] C. Beauchamp, I. Fridovich, A mechanism for the production of ethylene from methional. The generation of the hydroxyl radical by Xanthine oxidase, J. Biol. Chem. 245 (1970) 5214–5222, https://doi.org/10.1016/S0021-9258(18)62842-X.
[58] M. Hamadouche, A. Meunier, D.C. Greenspan, C. Blanchat, J.P. Zhong, G.P. L. Torre, L. Sedel, Long-term in vivo bioactivity and degradability of bulk sol–gel bioactive glasses, J. Biomed. Mater. Res. 54 (2001) 560, https://doi.org/10.1002/1097-4636(20010315)54:4<560::AID-JBM130>3.0.CO;2-J.
[59] M.L. Cooper, J.F. Hansbrough, Use of a composite skin graft composed of cultured human keratinocytes and fibroblasts and a collagen-GAG matrix to cover full-thickness wounds on athymic mice, Surgery 109 (2) (1991) 198–207. PMID: 1992553.
[60] W. Huang, M.N. Rahaman, D.E. Day, Y. Li, Mechanisms for converting bioactive silicate, borate, and borosilicate glasses to hydroxyapatite in dilute phosphate solution, Phys. Chem. Glasses: Eur. J. Glass Sci. Technol. B47 (2006) 647–658.
[61] O.L. Ranta, M. Vaahtio, T. Peltola, D. Zhang, L. Hupa, M. Hupa, H. Ylanen, J. I. Salonen, M.K. Viljanen, E. Eerola, Antibacterial effect of bioactive glasses on clinically important anaerobic bacteria in vitro, J. Mater. Sci. Mater. Med. 19 (2008) 547–551.
[62] T. Yao, Ju Chen, Z. Wang, J. Zhai, Y. Li, J. Xing, S. Hu, G. Tan, S. Qi, Y. Chang, P. Yu, C. Ning, The antibacterial effect of potassium-sodium niobate ceramics based on controlling piezoelectric properties, Colloids Surf. B Biointerfaces 175 (2019) 463–468, https://doi.org/10.1016/j.colsurfb.2018.12.022.
[63] Robert A. MacLeod, Esmond E. Snell, The effect OF related IONS ON the potassium requirement OF lactic acid bacteria, J. Biol. Chem. 176 (Issue 1) (1948) 39–52, https://doi.org/10.1016/S0021-9258(18)50999-6.
[64] Qiuquan Cai, Shuliang Yang, Chao Zhang, Zimeng Li, Xiaodong Li, Zhiquan Shen, Weipu Zhu, Facile and versatile modification of cotton fibers for persistent antibacterial activity and enhanced hygroscopicity, ACS Appl. Mater. Interfaces 10 (44) (2018) 38506–38516, https://doi.org/10.1021/acsami.8b14986.
[65] T.J. Beveridge, Structures of gram-negative cell walls and their derived membrane vesicles, J. Bacteriol. 181 (1999) 4725–4733, https://doi.org/10.1128/JB.181.16.4725-4733.1999.
[66] E. Kłodzinska, M. Szumski, E. Dziubakiewicz, K. Hrynkiewicz, E. Skwarek, W. Janusz, B. Buszewsk, Effect of zeta potential value on bacterial behavior during electrophoretic separation, Electrophoresis 31 (2010), https://doi.org/10.1002/elps.200900559, 1590–159.
[67] R. Sonohara, N. Muramatsu, H. Ohshima, T. Kondo, Difference in surface properties between Escherichia coli and Staphylococcus aureus as revealed by electrophoretic mobility measurements, Biophys. Chem. 55 (1995) 273–277, https://doi.org/10.1016/0301-4622(95)00004-H.
[68] M.T. Ehrensberger, M.E. Tobias, S.R. Nodzo, L.A. Hansen, N.R. Luke-Marshall, R. F. Cole, L.M. Wild, A.A. Campagnari, Cathodic voltage-controlled electrical stimulation of titanium implants as treatment for methicillin-resistant Staphylococcus aureus periprosthetic infections, Biomaterials 41 (2015) 97–105, https://doi.org/10.1016/j.biomaterials.2014.11.013.
[69] G. Harkes, J. Feijen, J. Dankert, Adhesion of Escherichia coli on to a series of poly (methacrylates) differing in charge and hydrophobicity, Biomaterials 12 (1991) 853–860, https://doi.org/10.1016/0142-9612(91)90074-K.
[70] Y. Liu, R. Qin, S.A.J. Zaat, E. Breukink, M. Heger, Antibacterial photodynamic therapy: overview of a promising approach to fight antibiotic-resistant bacterial infections, J. Clin. Transl. Res. 1 (3) (2015) 140–167.
[71] S. Kumar, R. Vaish, S. Powar, Surface-selective bactericidal effect of poled ferroelectric materials, J. Appl. Phys. 124 (2018), https://doi.org/10.1063/1.5024721.
[72] A.K. Dubey, B. Basu, Pulsed electrical stimulation and surface charge induced cell growth on multistage spark plasma sintered hydroxyapatite barium titanate piezobiocomposite, J. Am. Ceram. Soc. 97 (2014) 481–489, https://doi.org/10.1111/jace.12647.
[73] G.R. Sun, H. Li, X. Deng, C.P. Lau, Characterization of ionic currents in human mesenchymal stem cells from bone marrow, Stem Cell. 23 (2005) 371–382, https://doi.org/10.1634/stemcells.2004-0213.
[74] F. Ding, G. Zhang, L. Liu, L. Jiang, R. Wang, Y. Zheng, G. Wang, M. Xie, Y. Duan, Involvement of cationic channels in proliferation and migration of human mesenchymal stem cells, Tissue Cell 44 (2012) 358–364, https://doi.org/10.1016/j.tice.2012.06.001.
[75] M. Ohgaki, T. Kizuki, M. Katsura, K. Yamashita, Manipulation of selective cell adhesion and growth by surface charges of electrically polarized hydroxyapatite, J. Biomed. Mater. Res. 57 (2001) 366–373, https://doi.org/10.1002/1097-4636(20011205)57:3<366::AID-JBM1179>3.0.CO;2-X.
[76] C.J. Wilson, R.E. Clegg, D.I. Leavesley, M.J. Pearcy, Mediation of biomaterial–cell interactions by adsorbed proteins: a review, Tissue Eng. 11 (2005) 1–18, https://doi.org/10.1089/ten.2005.11.1.
[77] K.S. Hwang, J.E. Song, H.S. Yang, Y.J. Park, J.L. Ong, H.R. Rawls, Effect of poling conditions on growth of calcium phosphate crystal in ferroelectric $BaTiO_3$ ceramics, J. Mater. Sci. Mater. Med. 13 (2002) 133–138.